



EXPERIMENTAL INVESTIGATIONS ON AIRFOILS  
WITH DIFFERENT GEOMETRIES IN THE DOMAIN OF  
HIGH ANGLES OF ATTACK - FLOW SEPARATION

J. Keil

Translation of "Experimentelle Untersuchungen an Fluegeln  
verschiedener Geometrie im hohen Anstellwinkelbereich".  
Institut fuer Flugtechnik, Technische Hochschule Darmstadt ( Institute  
of Aeronautics, Darmstadt Technical University), Darmstadt, West Germany,  
March 16, 1984, pp. 1-89

LIBRARY COPY

SEP 10 1985

LANGLEY RESEARCH CENTER  
LIBRARY, NASA  
HAMPTON, VIRGINIA

NATIONAL AERONAUTICS AND SPACE ADMINISTRATION  
WASHINGTON, D.C. 20546 JULY 1985

1. Report No. NASA TM-77892	2. Government Accession No.	3. Recipient's Catalog No.	
4. Title and Subtitle EXPERIMENTAL INVESTIGATIONS ON AIRFOILS WITH DIFFERENT GEOMETRIES IN THE DOMAIN OF HIGH ANGLES OF ATTACK - FLOW SEPARATION		5. Report Date July 1985	
		6. Performing Organization Code	
7. Author(s) J. Keil		8. Performing Organization Report No.	
		10. Work Unit No.	
9. Performing Organization Name and Address The Corporate Word, Inc. 1102 Arrott Bldg. Pittsburgh, PA 15222		11. Contract or Grant No. NASW-4006	
		13. Type of Report and Period Covered Translation	
12. Sponsoring Agency Name and Address National Aeronautics and Space Administration Washington, DC 20546		14. Sponsoring Agency Code	
		15. Supplementary Notes Translation of "Experimentelle Untersuchungen an Fluegeln verschiedener Geometrie im hohen Anstellwinkelbereich," Institut fuer Flugtechnik, Technische Hochschule Darmstadt (Institute of Aeronautics, Darmstadt Technical University), Darmstadt, West Germany, March 16, 1984, pp. 1-89 (N84-33393)	
16. Abstract Wind tunnel tests were conducted on airfoil models in order to study the flow separation phenomena occurring for high angles of attack. Pressure distribution on wings of different geometries were measured. Results show that for three-dimensional airfoils layout and span lift play a role. Separation effects on airfoils with moderate extension are three-dimensional. The flow domains separated from the air foil must be treated three-dimensionally. The rolling-up of separated vortex layers increases with angle in intensity and induction effect and shows strong nonlinearities. Boundary layer material moves perpendicularly to the flow direction due to the pressure gradients at the airfoil; this has a stabilizing effect. The separation starts earlier with increasing pointed profiles.			
17. Key Words (Selected by Author(s))		18. Distribution Statement Unlimited	
19. Security Classif. (of this report) Unclassified	20. Security Classif. (of this page) Unclassified	21. No. of Pages 83	22. Price

N84-33393#  
(ORIGINAL)  
NASA-HQ  
N85-33110#<sup>2</sup>  
N-155,604

## Table of Contents

	Page
1. Symbols	5
2. Introduction	7
2.1 Survey of current research	7
2.2 Goal and procedure of this study	9
3. Wind tunnel measurements	10
3.1 Wind tunnel models	10
3.2 Data processing equipment for pressure measurement	11
3.3 Wind tunnel	12
3.4 Data processing	12
3.5 Test performance	12
3.5.1 Pressure distribution measurements	12
3.5.2 Colored pictures	13
4. Description of separation types taken from two-dimensional profile flow	15
4.1 Trailing edge separation	15
4.2 Leading edge separation	15
4.3 Short nose bubbles	16
5. Evaluation and discussion of measurement results of airfoils MF 1 to MF 5	17
5.1 MF 1; $\Lambda = 5$ , $\varphi = 0^\circ$ , $\lambda = 1$	18
5.1.1 Results of power measurements	18
5.1.2 Results of pressure distribution measurements	19
5.1.3 Results of coloring measurements to determine boundary layer pattern	20
5.1.4 Analysis of separation process	21

	Page
5.2 MF 2; $\Lambda = 5, \varphi = 30^\circ, \lambda = 1$	24
5.2.1 Results of power measurements	24
5.2.2 Results of pressure distribution measurements	25
5.2.3 Results of coloring measurements to determine boundary layer pattern	25
5.2.4 Analysis of separation process	26
5.3 MF 3; $\Lambda = 5, \varphi = 45^\circ, \lambda = 1$	28
5.3.1 Results of power measurements	28
5.3.2 Results of pressure distribution measurements	29
5.3.3 Results of coloring measurements to determine boundary layer pattern	30
5.3.4 Analysis of separation process	31
5.4 MF 4; $\Lambda = 5, \varphi = 30^\circ, \lambda = 0.5$	35
5.4.1 Results of power measurements	35
5.4.2 Results of pressure distribution measurements	35
5.4.3 Results of coloring measurements to determine boundary layer pattern	36
5.4.4 Analysis of separation process	37
5.5 MF 5; $\Lambda = 5, \varphi = 30^\circ, \lambda = 0.25$	37
5.5.1 Results of power measurements	37
5.5.2 Results of pressure distribution measurements	38
5.5.3 Results of coloring measurements to determine boundary layer pattern	38
5.5.4 Analysis of separation process	38
5.6 Summary of results of effect of layout parameter on separation behavior	39
5.6.1 Effect of sweep on separation behavior	39
5.6.2 Effect of taper ratio on separation behavior	42
5.6.3 Effect of flow field's three-dimensionality on separation behavior	43
6. Summary	44
7. References	46

1. Symbols

/1\*

A	Lift
b	Span
$C_A, C_{Amax.}$	Wing lift factor
$c_A, c_{Amax.}$	Local lift factor in a profile section $y = \text{const.}$
$c_m$	Local pitching moment factor in a profile section $y = \text{const.}$
$c_p, c$	Pressure factor, $c_p = 1 - \left(\frac{V}{V_{\infty}}\right)^2$
$C_W$	Wing resistance factor
$c_W$	Local resistance factor in a profile section $y = \text{const.}$
c	Induced resistance factor in a profile section $y = \text{const.}$
c	Pressure resistance factor in a profile section $y = \text{const.}$
d	Profile density
k	Disturbance density in a boundary layer trip edge
$k_x, k_y$	Dimensionless circulation distribution
$l_a$	Chord length at wing tip section
$l_i$	Chord length at wing root
$l_m$	Middle chord length
M	Mach number
Re	Reynolds number $Re = \frac{v \cdot l_m}{\nu}$
U, V, W	Mean flow velocities in directions x, y, z
W	Resistance
x, y, z	Cartesian coordinates
$\alpha$	Angle of attack
$\alpha$	Angle of attack at maximum lift
$\alpha$	Comparative angle of attack, definition see page (Page = Sheet 9)
$\eta$	Dimensionless span parameter $\eta = 2y / b$
$\Gamma$	Circulation
$\lambda$	Taper ratio $\lambda = \frac{l_a}{l_i}$

/2

---

\*Numbers in the margin indicate pagination in the foreign text.

$\Delta$

Aspect ratio

$\nu$

Kinematic viscosity

$\varphi$

Sweep

EXPERIMENTAL INVESTIGATIONS ON AIRFOILS  
WITH DIFFERENT GEOMETRIES IN THE DOMAIN OF  
HIGH ANGLES OF ATTACK - FLOW SEPARATION

J. Keil

2. Introduction

/3

If maximum lift is attained on a supporting surface (for example, aircraft wings), flow separation occurs as angle of attack increases. The processes are either no longer accessible or presently too complicated for a mathematical description (Navier-Stokes-solution).

Wind tunnel tests with wing models are used to determine and explain the separation process.

If aspect ratio  $\Lambda$  is left constant, the remaining layout parameter sweep  $\varphi$  and taper ratio  $\lambda$  affect separation behavior. Each effect on separation can be classified with a parameter variation.

2.1 Survey of current research

/4

The problem of separable flow on wings and profiles has been handled in the literature in the broadest sense by numerous authors. We shall first review two-dimensional profile flow.

Investigations on the effect of Reynolds number on pressure distribution at a profile NACA 4412 with large angles of attack are to be found in Pinkerton [10]. Gault [3] used a variety of measuring results to derive a widely used classification of different separation types independent of Re-number, profile density, and nose radius. While the aforementioned studies are limited to measurements of powers and pressure distribution at profiles, Seetharam and Wentz [4], as well as Young and Hoad [5]

investigate flow field surrounding a profile. Reference [4] emphasizes velocity distribution in the region of the trailing edge, while the velocity field inside and outside a separation bubble is determined in [5].

For wings of finite span, Kuechemann ([1] and [2]) developed flow models for separation types which are independent of airfoil layouts. In particular, he coined the expression: "part-span-vortex-sheet." This concept pertains to the rolling up of the vortex sheet in the area between adjacent and separated flow.

Models for separation processes were proposed and discussed in the studies by Hall [6] and Maskell [7], as well as very recently by Tobak and Peake [8], [9]. These studies may be grouped under the heading "Topology of Separated Flow." The models in the studies named attempt to shed light on the 5 interaction of separated vortex sheets with the wall boundary layer. For the most part, these fundamentally qualitative observations are based on investigations using different methods of making flow visible, particularly coloring processes to make boundary layers visible.

These types of investigations are found, for example, also in Werle [11], who investigates an arrowhead wing with variable sweep. This study also contains results taken from measurements in a smoke and a water tunnel. The process involved limits these types of investigations to very small Re-numbers.

Further measurements of pressure distributions on an arrowhead wing are found in Schmitt and Manie [12]. A part of these investigations were executed on a model whose layout and Re-number are similar to those of the arrowhead wing MF 3 (Figure 1) investigated in our study. This permits a comparison of the physical effects ascertained here.

Right-angle wings of moderate aspect ratio have received the most attention in the literature. Kohler [13], Jakob [14], Winkelmann and others [15], or Winkelmann [16] report on measuring results. I am not aware of any investigations which have a model system corresponding to the measurements underlying my study. The study by Lip and Schubert [17] investigates, on the one hand, only parameter sweep, although it does not measure high angles of attack at which flow separation begins.

Separation processes on the leading edge of thin delta 6 wings are discussed in numerous reports. Detailed representations are found, for example, in Hummel [18]. These studies interest us here since the results depicted there are also of use on wings considered in my study.

## 2.2 Goal and procedure of this study

The effect of layout parameter on separation processes is to be worked out through systematic analysis of power and pressure distribution measurements, as well as measurements with a coloring process to make the boundary layer visible on five airfoils of equal profile, with equal aspect ratio, but different sweep and taper ratio for angles of attack up to  $\alpha = 35^\circ$ . First, typical separation behavior of each individual airfoil is presented using typical and exemplary measuring results. I compare my results to similar measurements from other studies.

From the comparison of the results of the different airfoils themselves, I shall show that separation processes vary in their intensity and their effects on span lift distribution, apparently according to airfoil layout, while actually they are always based on similar physical mechanisms. For this reason, my investigation does not focus primarily on the condition of completely separated flow, but rather on the region of angle of attack, which stretches from the first local onset of flow separation to the formation of completely separated flow.

As an additional aspect, I shall consider to what degree <sup>/7</sup> separation types may be carried over from their two-dimensional flow field to the processes on a wing with its three-dimensional flow field.

### 3. Wind tunnel measurements

#### 3.1 Wind tunnel models

As already mentioned, a model system was chosen for the experimental investigations which would permit us to investigate the effect of layout parameter sweep  $\varphi$  and taper ratio  $\lambda$ . Common to all the model airfoils is an aspect ratio  $\Lambda = 5$  (Figure 1), as well as the profile NACA 0012. Each of the models prepared from GFK is equipped with pressure measuring pipes which reach from the center of the wing to the wing tip section and are positioned according to defined depth staggering (Figure 2). In sections  $\eta = \text{const.}$ , intended for measuring, the pipes are equipped with multiple measuring drills ( $d_B = 0.3 \text{ mm}$ ). For this reason, all borings which do not lie in the measuring section are sealed using a thin adhesive strip.

In order to minimize the effects of surface disturbances on the boundary layer, the wing nose is completely covered with a very wide adhesive foil. This keeps out all surface disturbances in span direction up to a chord length of  $x_i/l_m \approx 0.1$ . For  $x_i/l_m > 0.1$  each measuring section to be sealed is covered with a single adhesive strip (foil density  $k = 0.06 \text{ mm}$ ). These individual adhesive strips are applied in the direction of free oncoming flow. Since a small nose bubble forms on all five wings at angle of attack  $\alpha \geq 8^\circ$  (see also Chapter 4.3 regarding <sup>/8</sup> this), the boundary layer transition is set from laminar  $\rightarrow$  turbulent. The transition always takes place in the undisturbed area of the nose adhesive strips, a fact which can be seen by making the boundary layer visible.

In the region of the turbulent boundary layer, the adhesive strip has no effect on the boundary layer condition. For angles of attack  $< 8^\circ$  a transition from laminar to turbulent takes place without formation of a nose bubble. If, for an unfavorable situation, one starts from the fact that disturbance lies across the adhesive foil at a diagonal to the main flow direction, then the effect of the disturbance can be determined by the transition criteria, according to Kraemer [26]. Accordingly, an ineffective disturbance must correspond to the condition

$$\frac{U \cdot k}{\nu} \leq 10^2$$

With the velocity in the depth  $x_i/l_m = 0.1$  of approx. 60 m/s, one obtains  $\frac{U \cdot k}{\nu} \approx 240$ . This value is certainly higher than the boundary value (= 100; lt. [26]) given by Kraemer. Since only the cross-flow portion is actually disturbed, it can be assumed that no disturbance effect of the foil occurs. This type of minimum surface disturbance has no effect on separated flow.

Additionally, it must be noted, that separate placing of a pressure measuring pipe for every single measuring section using the aforementioned model dimensions was not compatible with the desired span measuring density.

### 3.2 Data processing equipment for pressure measurement

/9

The pressure tubes are connected to a measuring point switch with integrated pressure gauge. The data is at first analog, is then digitalized using a data processing device, and fed into a computer (Figure 3). In the computer, the intergration of the pressure distribution takes place "quasi-online" for calculating the local power and moment factors directly after measurements have been taken. A description of the device is found in [20].

The pressures to be measured take on a highly unstable character as separation begins. The device provides for multiple measurements at each measuring place in any amount desired and

at independently selectable time intervals between measurements in order to determine a representative average pressure factor (Figure 4). Measuring unstable pressure distributions is not possible with the available device, nor was it the goal of the investigation.

### 3.3 Wind tunnel

Measurements were carried out in the 3-m low-speed wind tunnel at the Institute for Flight Technology (since Oct. 1, 1982, Institute for Aerodynamics and Measuring Technology). This tunnel is a closed wind tunnel of Goettinger construction with open measuring section. It is described in [19]. The tunnel was suspended using the wire suspension of a six-component weighing lever with movable jockey. The same device was used for power measurements.

### 3.4 Data processing

/10

The data converted into pressure factors was transferred from the computer mentioned in 3.2 to the wind tunnel's PDP 11/40 computer and stored there on magnetic discs. The data was available for processing using various evaluation processes (for example, plotting pressure distribution, locally for a section  $\eta_i = \text{const.}$ , as well as over the entire span at all measuring positions; plotting local power and moment factors over the angle of attack, etc.).

### 3.5 Test performance

#### 3.5.1 Pressure distribution measurements

A measuring series of angles of attack, determined by the model construction, must be kept for measuring every measuring section (see also 3.1). All measurements were carried out continuously for increasing angles of attack, since the thematic

extent of the experimental studies is limited to onset and spread of flow separation. The hysteresis, ie., angle of attack difference between flow separation as angle of attack increases and reattachment with decreasing angle of attack, is not investigated.

Basically, one tries to use the wind tunnel for carrying out experiments with the highest possible Reynolds numbers to hold the difference to flight Reynolds number as low as possible. This is important since, in particular, the boundary layer is strongly dependent on the Re-number, a fact which substantially effects separation behavior. One of the Re-number boundaries /11 among the measuring results cited in my study, unfortunately, was caused by the wire suspension. If the load caused by the aircraft on the model suspension becomes too large, this causes resilience in the suspension. The unstable load character, in particular during the onset of separation, leads to marked model movements, which can cause changes in angle of attack. In such a case, we can no longer talk about a stationary situation. For this reason, all pressure distribution measurements were carried out at a Re-number of  $Re = 0.74 \times 10^6$  related to  $l_m = 0.28$ .

### 3.5.2 Colored pictures

~~Line Drawings~~ ?

~~Colored~~ pictures are frequently used in literature to make tangential wall stress patterns visible for qualitative description of flow processes. This was also mentioned in Chapter 2.1.

It must be mentioned, however, that in certain cases this measuring method presents problems for interpreting results. The problems arise from the test course. First, the colored airfoil is suspended on the measuring angle of attack for measurement and then placed in the wind tunnel flow. Since it is not possible to bring the air stream up to measuring speed spontaneously, the Re-number region of  $Re = 0$  to  $Re = Re_{Mess}$  will be traversed almost

in its entirety while the wind tunnel is accelerated. Airfoil flow conditions whose changes depend on Re-number are a part of this course. Since separation processes are more or less /12 subject to hysteresis, and boundary layer stability is less at smaller Re-numbers, the flow condition which actually corresponds to the angle of attack is not attained.<sup>1</sup>

With this, two measuring errors related to the process can occur during color picture measurements:

- a) In the case of wings on which the separation process occurs irregularly and only a small region of angle of attack is traversed before reaching complete separation, the colored pictures must be assigned to angles of attack smaller than the measuring angles of attack. (The assignment occurs on the basis of the comparison with the measured span pressure distributions). If these effects occur, a comparison angle of attack  $\alpha_{V_{cp}}$  is defined, which indicates which pressure distribution measurement angle of attack of the is to be compared with the colored picture.

The circumstance described in a) occurs mainly for MF 1 and, in part, also for MF 2.

- b) If wall tangential stress causes color to run even before the measuring Re-number is attained and another flow condition exists simultaneously, then many places on the airfoil will exhibit a colored picture which does not represent the measuring Re-number, since the color already took hold earlier and is no longer fluid.

---

<sup>1</sup>Usual procedure for measuring power and pressure distribution: For angle of attack  $\alpha = 0^\circ$ , wind tunnel is brought up to measuring flow speed. Measuring of the angle follows.

The effect described in b) is particularly observable on airfoil MF 3.

#### 4. Description of separation types taken from two-dimensional profile flow

/13

In the literature which deals with three-dimensional separation, it is common, as far as possible, to avail oneself of symbols used for processes involving comparable two-dimensional flow. For this reason, the most important separation types on a wing profile will be discussed first.

Besides Re-number and Ma-number, the influence parameters in two-dimensional considerations are limited to the profile parameters (profile density, curving, nose radius), while with three-dimensional considerations layout parameters (aspect ratio, sweep, taper ratio, and where necessary, angle of twist and dihedral) must also be taken into account.

##### 4.1 Trailing edge separation

On dense profiles ( $d/l > 15\%$ ) the boundary layer separates turbulently according to the transfer pattern laminar to turbulent as angle of attack increases on the trailing edge. The separation point moves steadily toward the leading edge with increasing angle of attack. At the onset of trailing edge separation, lift first increases further as the lift increase decreases. The course of the  $C_A$ - $\alpha$ -curve is flat in the area of maximum lift. Constant dead water pressure behind the point of separation characterizes pressure distribution for this separation type.

##### 4.2 Leading edge separation

/14

On thin profiles ( $d/l < 6$  to  $8\%$ ) the clearly defined collecting point, together with a subsequent, strong gradient,

leads to laminar separation on the leading edge already at small angles of attack ( $\alpha < 10^\circ$ ) in the pressure increase following the pressure minimum. The separated boundary layer transfers to the turbulent condition, whereby flow can build again. It forms a separation bubble. With the increase of the angle of attack, the reconstruction point moves to the trailing edge, whereby a constant pressure is established in the region of the separation bubble. Maximum lift is obtained when the bubble extends to the trailing edge. If the angle of attack is enlarged further, the bubble bursts, and a flow condition is obtained which is identical to the final condition of the type occurring with trailing edge separation (4.1). The bursting of the bubble expresses itself in the  $C_{L-\alpha}$ -path as an irregular lift decrease.

#### 4.3 Short nose bubbles

For moderately dense profiles ( $d/l \approx 8 - 15\%$ ) a separation mechanism occurs which is identical at first to leading edge separation. The separation bubble does not increase in length with the angle of attack, but rather displaces itself only at minimum pressure. After the short nose bubble has formed, two different flow forms may be observed:

- a) Upon reaching a boundary angle of attack, the bubble bursts and a condition of completely separated flow is attained. Bursting results in an irregular lift decrease.
- b) In addition to the short nose bubble, trailing edge /15 separation takes place. If the separation point of the trailing edge separation moves into the bubble, a fully separated flow condition is also established.

Mixtures of a) and b) are possible.

Figure 5 gives a detailed diagram of the  $C_A$ - $\alpha$ -pattern and a qualitative representation of resulting flow conditions and pressure distribution for the separation type described more briefly here.

In the diagram (Figure 6) compiled by Gault in [6] the separation type is based on the parameters of Re-number and nose radius (as equivalent to profile density). It shows that the parameters mentioned are well suited to provide a cut-off point and arrangement for an anticipated separation behavior.

#### 5. Evaluation and discussion of measuring results of airfoils MF 1 to MF 5

The following observations pertain primarily to the most important measuring results for each airfoil. These results will be represented and discussed. They are followed by comparisons made from observations of parameter sweep and taper ratio.

Finally, I attempted to identify generally valid physical mechanisms for flow condition of separated flow based on results from all five wings. Furthermore, I compare measurements taken from the literature (insofar as comparable results are available). The interaction of outer flow with boundary layer flow is shown using investigations on a boundary layer treated with colored tracer materials. Evaluation of measuring results concludes with a definition of different typical airfoil /16 separation structures. The classifying undertaken here is tested for possible agreement with known two-dimensional separation types.

In the following observations, measuring results will be used to discuss only the flight-specific peculiarities. If resulting separation effects are basically similar in form and, hence,

comparable, the comparable airfoil will be pointed out.\*

Reference [21] contains a systematic representation of the measuring results of the five airfoils. For reasons of clarity here all drawings and diagrams available in [21] and referred to in clarifying the processes involved in my study were not included in the picture portion. Instead, I have referred to the figure number in [21].

Further, only pressure distribution on the airfoil's /17 upper side is consistently considered in the following. Pressure distribution on the lower side is indeed affected by separation processes occurring on the upper side, however, no separation actually occurs on the lower side.

## 5.1 MF 1; $\Delta = 5, \varphi = 0^\circ, \lambda = 1$

### 5.1.1 Results of power measurements

The pattern  $C_A = f(\alpha)$  (Figure 1.1 in [21]), taken from the power measurements on the six-component weighing lever with movable jockey, shows linear lift increase with angle of attack up to approx.  $\alpha = 13^\circ$ . Thereafter, lift increase slightly reverses until maximum lift is attained at  $\alpha = 16.5^\circ$ . With continued angle of attack the lift factor reduces from  $C_A = 0.9615$  to  $C_A = 0.760$ . This measuring result already allows us to conclude that flow must be largely attached up until maximum lift is attained. Flow separation at  $\alpha > \alpha_{C_{A \text{ MAX}}}$  will expand over a

---

\*In the following, I use the terms: taper ratio of lift, lift distribution, maximum lift, etc. Since  $l_i = \text{const.}$  for all  $i$ ,  $A \sim C_A$  is valid. Therefore, to promote a more understandable formulation, correct designations, for example, "distribution of the lift factor", will not be used. Since  $l_i = f(\eta_i)$ , however, the correct designation will be used for tapered airfoils.

large portion of the airfoil (if not over the whole wing), since the  $C_A$  value changes only insignificantly after the lift reversal.

### 5.1.2 Results of pressure distribution measurements

Figure 1.2.1 in [21] shows span pressure distribution for  $\alpha = 4.5^\circ$  (measured from  $\eta = 0.04$  to  $\eta = 0.98$ ). The collecting point in the nose region is still relatively weakly defined. The pressure increase to the trailing edge following pressure minimum exhibits a decreasing gradient, which, however, does not /18 decrease to zero. This indicates a completely attached flow, just as does the small vacuum in the trailing edge region ( $c_{p_{HK}} > 0$ ). At  $\eta = 0.98$ , a second minimum pressure can be determined in the rear portion of the airfoil. This can be explained by the influence of the so-called tip vortex. Controlled by the pressure difference, the airfoil's side edge is flowed around (see also in [22] regarding this). The vortex sheet separates on the airfoil's side edge and rolls up into a so-called "bag vortex." This separation mechanism is comparable to that of the leading edge vortex on thin delta wings, which, for example, has been investigated in detail by Hummel in [18].

At  $\alpha = 12.5^\circ$ , the collecting point forms markedly in the nose region (Figure 1.2.4 in [21]). Shortly after pressure minimum, a nearly constant pressure can be determined on two consecutive measuring points. This pressure pattern indicates the presence of short nose bubbles (see 4.3).

The pressure distribution for  $\alpha = 16.5^\circ$  (Figure 1.2.6 in [21]) corresponds to the flow condition directly before attaining  $C_{A_{MAX}}$ . The intense induction effect of the tip vortex is particularly notable.

The pressure on the trailing edge of the wing's upper side is an important indicator which shows on which part of the wing flow separation will begin first. In this instance, a pressure decrease signals the growth of the boundary layer in the trailing edge region and/or the first onset of separation.

Figure 7 shows the pattern  $c_{P_{HK}} = f(\eta, \alpha)$  for angle of 19 attack  $\alpha < \alpha_{C_{A_{MAX}}}$ . One recognizes that due to pressure decreases in the wing's mid span section, the first onset of separation is likely to occur there. The correctness of this prognosis is proven by measurements for angle of attack  $\alpha > \alpha_C$ . At  $18.0^\circ$ , the area from the wing's mid span up to  $\eta = 0.8$  separates to a large extent (Figure 1.27 in [21]). In the region  $\eta = 0.1$  to  $0.3$  a residual collecting point remains which indicates that the separation there does not immediately follow on the wing nose. The flow is completely separated at  $\alpha = 24^\circ$  (Figure 1.2.12 and ff. in [21]).

Figure 8 shows the pattern of the span lift distribution for the angles of attack mentioned.

### 5.1.3 Results of coloring measurements to determine boundary layer pattern

As the colored picture shows, at angles of attack  $\alpha = \alpha$

= 4°, the boundary layer still has a predominantly two-dimensional character. Cross-flow is almost negligible (Figure 9). The flow around the tip lobe affects the boundary layer solely in the immediate region of the wing tip. The cross-flow tendency can be clearly recognized in the rear portion. Cross-flow emanates from the tip vortex rolling up over the wing's side edge.

The alteration of the fine structure in the nose region indicates the transfer region from laminar to turbulent boundary layer. The short nose bubble, as shown, is not only detectable using pressure distribution, but also highly detectable using the coloring process.

Separation and reattachment lines are clearly visible in Figure 10 ( $\alpha = 10^\circ$  for  $\alpha_{V_{c_p}} = 12^\circ$ ). Figure 13 shows the flow mechanism which causes this color distribution.

First beginnings of trailing edge separation, as they can be predictable from the trailing edge pressure pattern, are clearly visible in Figure 10 ( $\alpha = 13^\circ$  for  $\alpha_{V_{c_p}} = 15^\circ$ ). One recognizes a definite dividing flow line at  $x_i/l_m \approx 0.85$ . Upon further increasing angle of attack to  $\alpha = 14^\circ$  ( $\alpha_{V_{c_p}} \approx 17^\circ$ ), flow in the wing's mid-span section separates to a large extent (Figure 11). With the exception of flow around the tip, the boundary layer moves into a vortex-like area. This structure is called "owl's eyes" [23] or "mushroom" [9]. If angle of attack increases further, the vortex core moves to the wing tip. At angles of attack  $> 20^\circ$ , the vortex core is in the nose region of the wing tip (Figure 12). The colored picture at  $\alpha = 20^\circ$  is interesting, as well, since the boundary layer structure exhibits well-defined cross-flow areas.

#### 5.1.4 Analysis of separation process

In order to initiate flow separation on a three-dimensional

airfoil, two parameters of influence are primarily involved:

- a) the maximum of local lift distribution, and
- b) local build up of boundary layer material.

The lift maximum for the straight right-angle wing lies in the wing's mid-span section. Since the span circulation /21 gradient is very small at this point, flow in this region is designated as very nearly even. This is the reason why the wing's mid-span section is where separation must begin. The span pressure gradient is directed toward the center of the wing and impedes removal of boundary layer material in this region. Measuring results given in 5.1.2 verify the depicted state of affairs. The parameter of influence a), described above, is, however, no longer applicable for the continued spreading of separation. After flow in the wing's mid-span section has reached a maximum lift load and is interrupted, the lift factor  $C_A$  decreases sharply for the straight right-angle wing. It is first necessary to consider some typical airfoil characteristics in order to understand the spreading behavior of separation.

An essential difference between three-dimensional airfoil flow and two-dimensional profile flow exists in alterable span circulation distribution and cross velocity connected with it. Based, for example, on the wing theory according to Truckenbrodt [22], these velocities may be calculated at:

$$v = \pm \frac{1}{2} k_x ; \text{ wobei } k_x dy = \frac{dr}{d\eta} \cdot d\eta \quad (5.1)$$

From this it is immediately clear, that the three-dimensional character (that is, a cross velocity  $v < u$ , but  $v \neq 0$ ) must be present most strongly in areas with accentuated span circulation gradients. For unseparated flow condition, this recognized state of affairs expresses itself in flow around the airfoil tip and in the tip vortex caused by it. Furthermore, as the colored pictures show, a corresponding cross-flow component forms in the boundary layer. Cross-flow resulting from a span circulation /22

gradient occurs, however, not only with attaching flow, but also for partial and complete separation condition. Two areas with well-defined circulation gradient can be ascertained on the lift distribution for  $\alpha = 18.0^\circ$ :

- a) the airfoil tip region, as well as
- b) the region at  $\eta = 0.2$  to  $0.3$ .

Figure 14 shows a possible model of the flow condition which occurs and is also correlated to the corresponding colored picture (Figure 1). In the separation area at the attaching flow, the separated vortex sheet rolls up into a bag vortex-like structure. The tip vortex is found on the airfoil tip. With increased angle of attack, the inner vortex area moves towards the airfoil tip. In contrast to Figure 11, the placement is recognizable in Figure 12. Pressure distribution produces pressure factors  $c = \text{const.}$  for  $\eta_i = \text{const.}$  for completely separated flow condition, however, not for all  $\eta_i$ , that is, the pressure distribution locally has a typical dead water pattern. It remains, however, a well-defined span pressure gradient. This pressure gradient (and with it, also, circulation gradient) originates from the described flow behavior, particularly in the occurrence of cross-flows which are concentrated in vortex structures.

Now we may apply this knowledge to the spreading behavior of flow separation on the straight rectangular wing. The flow pattern already described in Figure 14 influences the boundary layer, in that boundary material is transported from the 23 trailing edge region of the still attached area (outer airfoil) into the separated area of the wing's mid-span section. The boundary layer here cannot flow away and, for this reason, must expand, which brings about a spreading of the separated area. This behavior is clearly verified using the colored pictures already introduced. This behavior of the outer flow and the boundary layer has a basically destabilizing character here.

For this reason, too, unlike the wing's mid-span section, local maximum lift is determined in the other regions (Figure 1.8 in [21]).

The local maximum lift for  $\alpha = 30^\circ$  (Figure 8) corresponds nearly exactly to the lay of the vortex center in Figure 12.

From these results, it can be derived, that even at complete separation, flow is substantially affected by three-dimensional effects.

## 5.2 MF 2; $\Lambda = 5$ , $\varphi = 30^\circ$ , $\lambda = 1$

### 5.2.1 Results of power measurements

Maximum lift was measured at  $\alpha = 18.5^\circ$  for the wing with sweep of  $\varphi = 30^\circ$ . As  $\alpha$  increases,  $C_A$  decreases only slightly at first. Only at approximately  $21.5^\circ$  does the lift reduce irregularly to  $C_A \approx 0.1$ . The rest of the lift reversal is then regular once again (Figure 2.1 in [21]). Already the different  $C_A$ - $\alpha$ -pattern for MF 1 indicates definite changes in separation behavior. Similar to MF 1, the linear range of the  $C_A$ - $\alpha$ -pattern stretches to  $\alpha \approx 12^\circ$ .

/24

### 5.2.2 Results of pressure distribution measurements

As with the straight rectangular wing, two flow effects in the pressure distribution can be observed on the arrowhead wing MF 2 for the condition of fully attached flow (Figures 2.2.1, 2.2.4, 2.2.7 in [21]):

- a) Lay and spread of a short nose bubble for angle of attack  $\alpha > 8^\circ$ , and
- b) Influence of tip vortex on pressure distribution in the outer section ( $\eta = 0.98$ ).

Up to  $\alpha = 18.5^\circ$ , flow is to a large extent completely attached. Trailing edge pressure (Figure 13) has decreased more markedly in the center wing region. Accordingly, separation can be anticipated there. The arrowhead wing separates in two stages, as pressure distributions for a further increase of the angle of attack show.

At  $\alpha = 19^\circ$ , the outer region of  $\eta = 0.6$  to  $\eta = 1.0$  separates spontaneously. At  $\alpha \approx 21.0^\circ$ , the remaining portion of the wing separates. This second separation is connected to the marked lift reduction in the  $C_A$ - $\alpha$ -curve (Figure 2.1 in [21]). A remaining collecting point still present in the wing's mid-span section at  $\alpha = 21.5^\circ$  breaks down during further increase of angle of attack (Figure 2.2.8, 2.2.10, 2.2.14 in [21]).

Locally comparable to MF 1, the flow has a typical dead water character for the completely separated condition, whereby the dead water pressure over the span, however is not constant either.

### 5.2.3 Results of coloring measurements to determine boundary layer pattern

With the angle of attack  $\alpha = 8^\circ$ , the short nose bubble is evident, and the area of the tip vortex effect is clearly recognizable (Figure 16). An area with local trailing edge separation comes about and spreads out for the angle of attack range of  $12^\circ$  to  $18^\circ$ . Figure 19 shows the lay of the separation flow line which is dependent on angle of attack. A separation flow line of nearly constant density is obtained in the outer wing. The trailing edge separation which occurs does not express itself in a pure reverse flow as is the case for two-dimensional flow, but rather in a combined reverse-cross-flow of the wing's trailing edge. In this situation the direction of movement is towards the wing tip.

The flow in the outer region of the airfoil separates with  $\alpha = 18^\circ$ . In the corresponding colored picture (Figure 18) one recognizes a vortex core at  $\eta = 0.5$ . Figure 18 could give rise to the impression that suspension in section  $\eta = 0.5$  is responsible for the lay of the vortex center. This agreement is a chance one. Investigations provided no evidence, particularly for the positioning of the vortex center which is dependent on angle of attack (see also Figure 25 regarding this), indicating such a marked suspension interference.

This vortex core moves to the wing's mid-span section for  $\alpha_{V_{cP}} = 19^\circ$   $\hat{=} \alpha = 21^\circ$  and is still evident there for  $\alpha_{V_{cP}} = 28^\circ$  (Figure 18).

Accordingly, based on the results cited here, four condition ranges may be defined for the arrowhead wing MF 2:

- |    |                                   |   |           |
|----|-----------------------------------|---|-----------|
| a) | $\alpha < 10^\circ$               | no local separation area<br>no reverse flow   | <u>26</u> |
| b) | $\alpha = 12^\circ$ to $17^\circ$ | local trailing edge separation, clearly defined reverse-cross-flow emanating from trailing edge in separation area  |           |
| c) | $\alpha = 18^\circ$ to $21^\circ$ | Vortex center at $\eta = 0.5$ , inner wing still attached, outer wing fully separated, clearly defined reverse flow |           |
| d) | $\alpha = 22^\circ$               | Vortex center at $\eta = 0.05$ , wing to large extent completely separated  |           |

#### 5.2.4 Analysis of separation process

Upon observing the separation process on the MF 2, the first question which occurs is whether the criteria cited in 5.1.4 can also be used here for initiating separation processes. Local

maximum lift at  $\eta \approx 0.5$  is obtained from span lift distribution at  $\alpha = 18^\circ$  (Figure 2.7.2 in [21]). Here we see a well-known sweep effect on lift distribution: Lift maximum moves from the wing's mid-span section to the outside. Separation of the outer wing region beginning from  $\alpha > 18.5^\circ$  does not agree with the lift criterion. We know from pressure distributions and colored pictures that separation processes already occur in the outer region in the form of local trailing edge separation. Colored pictures clearly indicate transport of boundary layer material from the wing's center to the outer wing. At  $\alpha = 18^\circ$ , trailing edge separation in the airfoil's outer portion has expanded /27 to  $x_1/l \approx 0.4$ . For this reason, it is logical with regard to the boundary layer condition to expect flow separation in this wing part as angle of attack increases. For flow around the inner region of the wing no change occurs in transport direction in the boundary layer region due to separation processes in the outer portion of the wing. It can even be anticipated that the vortex structure which forms at first stabilizes the boundary layer by intensifying the cross movement (as, for example, MF 1 shows: marked  $\Gamma$  gradient in the separating area between attaching and separated flow with formation of a vortex system having markedly local cross velocities).

As the span lift distribution at  $\alpha = 19$  shows, a considerable lift gradient (and with it a circulation gradient) is present (Figure 2.7.2 in [21]). The inducing effect and ramification of this vortex system is shown most clearly with  $c_A$ - $\alpha$ -curves for  $\eta = 0.3, 0.4, \text{ and } 0.6$  (Figure 20).

The separation occurring in the outer region is signaled by lift reversal at  $\eta = 0.6$ . Lift for  $\eta = 0.3$  and  $0.4$  increases markedly with separation in the outer region. The vortex system which occurs apparently induces additional cross velocities on the wing's upper side and, connected to that, an additional vacuum, which, for its part, results in a lift increase. This flow behavior may be compared with behavior of leading edge

vortices on slim delta wings. Particularly the  $c_A$ - $\alpha$ -curves exhibit a comparable pattern.

The aforementioned comparison with separation processes /28 on the leading edge of slim delta wings primarily relates only to the  $C_A$ - $\alpha$ -curve pattern in the mentioned airfoil sections of the MF 2. The ascertained local lift behavior cannot be gathered directly from the measured pressure distributions.

Separation of the wing's inner portion at  $\alpha = 21^\circ$  can probably be attributed to the very high lift load in this region.

The lift factor decreases from the wing's mid-span section to its tip in the span lift distribution for  $\alpha = 22^\circ$ . The local maximum is located at the position of the vortex center (Figures 2.7.3, 2.7.4 in [21]). As with MF 1, there apparently exists a direct dependence between lift distribution during completely separated flow and lay of the vortex structure at hand.

### 5.3 MF 3; $\Lambda = 5$ , $\varphi = 45^\circ$ , $\lambda = 1$

#### 5.3.1 Results of power measurements

As sweep increases to  $\varphi = 45^\circ$ , the  $C_A$ - $\alpha$ -pattern changes radically in comparison to the patterns witnessed on MF 1 and MF 2. One is struck by the nearly constant lift increase  $C_{A\alpha}$  up to  $\alpha \approx 18^\circ$  (Figure 3.1 in [21]). The measured lift maximum is very flat,  $C_A$  is nearly constant up to  $\alpha = 30^\circ$ . The angle of maximum lift ought to lie at  $\alpha = 22^\circ$  to  $25^\circ$ . In spite of this very high angle of attack, almost the same maximum lift is obtained as on the MF 2. Similar to MF 2, the  $C_A$ - $\alpha$ -pattern from the power measurement on MF 3 does not permit any guaranteed statement on separation behavior.

For the swept wing with  $\varphi = 45^\circ$ , just as with both of the wings MF 1 and MF 2, for angles of attack  $\alpha < 14$  we observe the short nose bubble, on the one hand, while at the same time we recognize the influence of the tip vortex, as well. In the tip vortex region smaller additional vacuums are induced. At  $\alpha = 16.5^\circ$ , pressure distribution changes in the trailing edge region (Figure 3.2.7 in [21]). A pressure decrease and the decrease of wing tip vacuums induced by tip vortex indicate beginning trailing edge separation. At  $\alpha = 18.5^\circ$ , (Figure 3.2.9 in [21]), a "vacuum mountain" has formed in the rear portion of the wing in the region  $\eta = 0.4$  to  $0.8$ . At the same time, the area in the wing tip region affected by trailing edge separation expands. Span pressure distribution still exhibits flow around the nose at the collecting point up to the angle of attack mentioned last. This collection point breaks down with an increase of angle of attack to  $\alpha = 20.5^\circ$  in the region  $\eta = 0.8$  to  $1.0$  (Figure 3.2.11 in [21]).

The vacuum area already mentioned becomes stronger. Simultaneous with the formation of this marked pressure distribution, local  $c_A$ - $\alpha$ -curves in the corresponding span positions exhibit a markedly increasing lift (Figures 3.3.1 to 3.3.3 in [21]). As the angle of attack increases further, pressure distribution develops as follows:

The area with completely separated flow (characterized by the constant dead water pressure in the corresponding measuring section, as well as by the collecting point which is no longer present) expands to the wing's mid-span section. The vacuums in the vacuum area designated as a "vacuum mountain" increase. Furthermore, a movement toward the mid-span section of the wing begins. /30

The alteration of this markedly "unusual" pressure distribution, which is dependent on angle of attack, is not easily interpretable using the given plots of span pressure distribution. A better insight into alteration behavior of pressure distribution dependent on angle of attack was obtained in [24] using a trick film, which presents the change of pressure distribution in its dependence on angle of attack (as a time parameter). (Detailed references to this are made in 5.3.4.)

In contrast to the arrowhead wing MF 2, pressure distribution on MF 3 at  $\alpha = 29.5^\circ$  does not display an equal, typically dead water pressure pattern over the entire span. At  $\eta = 0.05$ , one still recognizes a well-defined collecting point (Figure 3.2.16 in [21]).

### 5.3.3 Results of coloring measurements to determine boundary layer pattern

A short nose bubble developed on the arrowhead wing even at  $\alpha = 6^\circ$  (Figure 21). Further, it can be ascertained that the boundary layer in the trailing edge region exhibits a well-defined cross component to the wing tip.

At  $\alpha = 10^\circ$ , an area with trailing edge separation forms over the entire span. It is characterized by the clearly visible separation flow line (Figure 22).

The boundary layer in this area flows constantly across /31 the flow direction. The separated area expands to the leading edge as angle of attack increases. Lay of the separating flow line and flow direction of the boundary layer are dependent on angle of attack (up to  $\alpha = 16^\circ$ ). They may be seen in Figure 24.

At  $\alpha = 17^\circ$ , the outer portion of the wing up to  $\eta = 0.65$  separates completely (Figure 23). In the position at which the separating flow line now meets the leading edge, a vortex

structure forms, just as was the case with wing MF 2. As angle of attack continues to increase, the center of this vortex moves gradually (not irregularly as with MF 2) toward the wing's mid-span section.

Figure 25 shows the displacement which is dependent on angle of attack. At  $\alpha = 28^\circ$ , the vortex structure is located in the mid-span section of the wing. The boundary layer located behind the vortex center in direction of flow has pure cross-flow character.

#### 5.3.4 Analysis of separation process

Pressure distributions and local power factors derived from them on the MF 3 are the most notable results of the investigated wing system. Three items are particularly interesting:

- a) For angle of attack  $\alpha > 16^\circ$ , an additional vacuum area develops behind the wing portion. Pressure distributions for this area at certain span sections and certain angles of attack exhibit a pattern which may be compared with a pressure distribution induced by a tip vortex (Figure 26). Such pressure distributions cannot be /32 attributed to two-dimensional separation types with their corresponding typical pressure distributions.
- b) All local  $c_{A\alpha}$ -curves in the region  $\eta = 0.05$  to  $0.8$  exhibit an increase of  $c_{A\alpha}$  before reaching  $c_{A\max}$ .
- c) Local  $c_{A\max}$  values are measured in the direction of the wing's mid-span section. These values lie far above the profile -  $C_{A\max}$  value of the NACA 0012 profile (Figure 3.8 in [21]). The same is true for  $\alpha_{c_{A\max}}$  (Figure 3.9 in [21]).

Similar to that of the more weakly swept wing MF 2, flow separation moves, on the one hand, motivated by strong cross-flows and the transport of boundary layer material connected to it, toward the wing tip. On the other hand, it moves away from the wing's mid-span section (in contrast to the straight rectangular due to displacement of span lift maximum. Initiated by these parameter conditions, first an area with trailing edge separation occurs in the region of the wing tip, whereby the line of separation has about the sweep of the leading edge.

This still very weakly defined separation area already displays the tendency of vortex sheet roll-up. This conclusion results from the decrease of pressure in the trailing edge region at  $x_i/l \approx 0.7$  to  $0.9$  (Figure 3.2.7 in [21]), whereby the pressure decrease may be seen as the result of additional velocities induced by the rolling up process. The developing flow field is sketched in Figure 27.

As angle of attack increases from  $\alpha = 10^\circ$  to  $\alpha = 16^\circ$ , the 33 separation line moves toward the leading edge. At  $\alpha > 16$ , flow of  $\eta = 0.7$  to  $\eta = 1.0$  is completely separated from the leading edge.

In the colored picture (Figure 23) we observe the formation of a vortex area on the leading edge at  $\eta = 0.7$  for  $\alpha = 17^\circ$ . Unaffected by the separation process in the region of the wing tip, the separation line remains in the region of the wing's mid-span section. As already mentioned, a well-defined vacuum area develops simultaneously in the rear portion of the wing. Apparently, the rolling up processes intensify in the separated vortex sheet, and the induced additional velocities intensify, as well.

The comparison of the rolling up process of the leading edge vortex on a slim delta wing, which is derived from the similarity of pressure distribution and local lift characteristics,

represents the starting point for a physical model of the flow process.

If one looks at the measuring results thusly, it can be considered insignificant whether separation of the vortex sheet results on a sharp leading edge from flow around it, or if the vortex sheet on the arrowhead wing separates along a separation line on the wing's upper side as the result of stability in the boundary layer. The important parameter for the formation and comparability of these processes is the sweep of the separation line. Strong circulation gradients occur through sweep and spatial separation of the vortex elements connected to it (for a model idea, which replaces the airfoil by a horseshoe vortex distribution in span and depth direction). These gradients /34 generate a downwash field which results in a well-defined rolling up of the separated vortex sheet.

The measuring results of Schmitt and Manie [12] provide evidence that flow processes involve to a large extent typical layout characteristics. Their investigations are based on a wing half model with layout parameters  $\varphi = 50^\circ$ ,  $\Delta = 5$ ,  $\lambda = 1$ , profile ONERA "D", measured at  $Re = 0.84 \times 10^6$ . The pressure distribution represented in Figure 28 exhibits a comparable pattern (typical "vacuum mountain").

The missing collecting point on the wing nose is apparently a result of the profile type, which, in comparison to the NACA 0012 profile, exhibits a density of only 10.5%. A further proof that the given flow process cannot involve the formation of a dead water area, is shown by the transfer of  $c_w$  over  $c_A^2$  in sections  $\eta = 0.2$  and  $\eta = 0.4$  (Figure 29). The separation process can be recognized in this type of representation by the deviation of the data from curve patterns which are originally straight. If a  $c_w$  value occurs, which is out of proportion to the corresponding  $c_A^2$ , then this is the result of the increase in the proportion of pressure resistance caused by separation and the dead water

area arising from it ( $c_w = c_{w_i} + c_{w_p}$ ; for pressure distribution measurements).

In Figure 29 we see that, at  $\alpha = 25.5^\circ$  (for  $\eta = 0.2$ ), the values still lie on the linear portion of the curve. At the same time the corresponding pressure distribution clearly shows the second vacuum area in the rear portion of the wing.

Although significant similarities in the type of flow around the wing arose from the comparison with flow processes on a slim delta wing, nonetheless one important difference to the arrowhead exists. The formation of a rolled-up, separated vortex sheet is dependent on angle of attack in its position on the airfoil and in the intensity of additional induction. The lay of the separating line is not fixed on the leading edge, as is the case with the delta wing, but rather dependent on condition of the wing boundary layer. In the trick film from [24], already mentioned above, this becomes particularly clear. As angle of attack increases, the vacuum area in the region of the rear portion of the wing moves toward the wing center in waves. Furthermore, it is shown that the growth of the completely separated area in the wing's outer portion does not weaken the intensity of the vortex sheet rolling up in the inner portion, but rather, if need be, strengthens it more. This possible intensification results, much as we have seen to be the case in 5.2.4 for the MF 2, from circulation gradients between the completely separated outer portion of the wing and the rest of the airfoil. Keeping this consideration in mind, a flow field can be assumed, which, for example, could have the pattern drawn in Figure 30 (valid for angles of attack of  $17^\circ$  to  $23^\circ$ ).

Two separation conditions occur during the flow condition seen in the sketch. Apparently, the separated vortex sheet rolls up in the wing's inner section. In the outer portion of the wing, on the other hand, the flow has a dead water character. While the former separation form, to a large extent, causes no

increase in pressure resistance, and the given flow, by all means, still would permit theoretically potential consideration (and, as such, be calculable), the dead water structure /36 causes an increase in pressure resistance and a marked impulse loss in the flow. The flow condition is difficult to describe using these differences. It cannot be said for sure (on the basis of the information available from the present measurements), whether, as is represented in Figure 31, an additional rolling up process develops in the separation area between the two flow forms. This state of affairs can be clarified only by measuring the velocity field. No such measurements, however, are to be found in the literature. Werle's quite detailed investigations [11] in a water and a smoke tunnel very perceptibly show flow behavior in relation to separation behavior at variable sweep, however, the Reynolds numbers of the investigated flow conditions are 20 times smaller than the Re-numbers in the measurements here. This state of affairs prohibits a comparison.

#### 5.4 MF 4; $\Delta = 5$ , $\varphi = 30^\circ$ , $\lambda = 0.5$

##### 5.4.1 Results of power measurements

The  $C_A$ - $\alpha$ -pattern measured for the weakly ( $\lambda = 0.5$ ) tapered arrowhead wing is basically similar to the pattern of the untapered arrowhead wing MF 2 (equal sweep  $\varphi = 30^\circ$ ). The taper ratio has an apparently comparable affect on separation behaviors (Figure 4.1 in [21] in comparison to Figure 2.1 in [21]).

##### 5.4.2 Results of pressure distribution measurements /37

The taper ratio for the wing MF 4 changes from that of the MF2 from  $\lambda = 1.0$  to  $\lambda = 0.5$ . As the taper ratio increases, similar to the case with increasing sweep, the span  $C_A$  maximum moves toward the wing tip and simultaneously increases.

From the measured pressure distributions it may be gathered that flow up to  $\alpha = 16.5^\circ$  completely attaches ( Figure 4.2.6 in [21]).

As with both arrowhead wings, MF 2 and MF 3, we recognize that trailing edge separation in the region of the wing tip is indicated by a pressure decrease and, for that reason, separation processes may be expected there in greater number.

At  $\alpha = 17.5^\circ$ , the flow in the region  $\eta = 0.8$  to  $\eta = 0.9$  is separated to a large extent (Figure 4.2.7 in [21]). In the wing tip region from  $\eta = 0.9$  to  $\eta = 1.0$  a stable flow around the nose still maintains itself at first, a fact which is clearly recognizable by the well-defined collection point. This region breaks up, too, with an increase to  $\alpha = 18.5^\circ$ . The completely separated area spreads out toward the wing's mid-span section in the region of angle of attack alteration from  $\alpha = 18.5^\circ$  to  $\alpha = 24.5^\circ$  (Figure 4.2.8 to 4.2.12 in [21]). Flow is considered completely separated for  $\alpha = 26^\circ$ .

Induction effects from separated vortex sheet roll-up, are not at first immediately recognizable from the pressure distributions, as is also the case with MF 2. It is necessary to refer to the local  $c_A$ - $\alpha$ -curves (Chapter 5.4.4).

#### 5.4.3 Results of coloring measurements to determine boundary layer pattern

/38

The colored pictures on MF 4 indicate typical characteristics, similar to the colored pictures of MF 2 and MF 3. Easily recognizable is the well defined cross-flow, particularly in the rear portion of the wing (Figure 32). At  $\alpha = 14^\circ$ , trailing edge separation in the wing's outer region can be recognized by the separating flow line (Figure 33). The colored pictures of  $\alpha = 16^\circ$  to  $\alpha = 22^\circ$  are defined by the vortex area forming in the separating area between attaching and separated

flow (for example, Figure 34). The uniformity of the separation behavior is shown by the application of vortex cores over the angle of attack (Figure 25).

The colored picture at  $\alpha = 30^\circ$  (Figure 35) clearly shows that a flow field with an aligned character exists also for the completely separated condition. The color, and with it also the wall tangential stress, is clearly spread over the entire wing surface.

#### 5.4.4 Analysis of separation process

The wing MF 4 possesses the same quarter chord line sweep as the MF 2. As measuring results show, altering the taper ratio (in comparison to MF 2) caused almost no change in separation behavior.

The vortex area which we see in the colored pictures for  $\alpha = 16^\circ$  indicates a rolling up process of the separated vortex sheet. This is verified by the local  $c_A$ - $\alpha$ -curves. An increase of  $c_{A\alpha_i}$  may be determined before reaching local maximum lift in most measuring sections  $\eta_i$  (Figures 4.3.1 to 4.3.3 in [21]). From 39 this it may be assumed that a condition comparable to that for the MF 2 occurs in the flow field. For this reason, we can refer to the detailed information in 5.2.4. The effect of the taper ratio will be discussed and explained in detail in Chapter 5.6.2.

### 5.5 MF 5; $\Lambda = 5$ , $\varphi = 30^\circ$ , $\lambda = 0.25$

#### 5.5.1 Results of power measurements

Altering taper ratio to  $\lambda = 0.25$  yields a further comparison of the  $C_A$ - $\alpha$ -pattern and a broader lift maximum.  $C_{Amax}$  is measured at approx.  $\alpha = 19^\circ$ . The absence of any and all irregularities in lift characteristics up to angles of attack of  $\alpha = 30^\circ$  indicates very even separation behavior (Figure 5.1 in [21]).

### 5.5.2 Results of pressure distribution measurements

In contrast to MF 4, lift load in the wing's outer region continues to increase with the taper ratio, since  $c_A$  ( $\alpha = \text{const.}$ ) increases there (Figure 5.2.3 in [21]). As a result flow separates on the wing tip already at  $\alpha = 13.75^\circ$  (Figure 5.2.5 in [21]). The separation area expands from  $\alpha = 14^\circ$  to  $\alpha = 26^\circ$  evenly up to the wing's mid-span section. Peculiarities in pressure distributions inside the named angle of attack region are not ascertainable (Figures 5.2.6 to 5.2.13).

### 5.5.3 Results of coloring measurements to determine boundary layer pattern

/40

Seen from the output dependent on angle of attack, the colored pictures on MF 5 are very similar to the results of MF 4. The site alteration of the vortex center for MF5 stretches over a larger angle of attack region (Figure 25). Accordingly, the separation process takes place more evenly than with MF 4, a fact which is already recognizable from pressure distributions.

Nonetheless, a peculiarity with smaller angles of attack must be mentioned. At  $\alpha = 8^\circ$ , the short nose bubble (which for wings MF 1 to MF 4 developed over the entire span) developed only in the region  $\eta = 0.4$  to  $\eta = 1.0$  (Figure 36). Further inside, the color structure indicates alteration solely of boundary layer condition--the transfer from laminar to turbulent. This result is expected according to the diagram given by Gault (Figure 6), since local Re-number increases also with local depth on the airfoil so that flow no longer tends toward separation.

### 5.5.4 Analysis of separation process

Basically, the separation processes of wings MF 2, MF 3, and MF 5 are alike. One difference is apparent on MF 5, insofar as

the separation process covers a very large angle of attack region from the first appearance of completely separated areas until the complete separation over the entire wing surface.

The complete separation of the leading edge in the wing /41 tip region already at  $\alpha = 13^\circ$  is caused by high  $c_A$  load in this portion of the wing determined by taper ratio. The application of  $c_{Amax}$  over  $\eta$  (Figure 5.8 in [21]) verifies that the onset of flow separation cannot be predicted by comparing local  $c_{Amax}$  with two-dimensional  $C_{Amax}$  values (in accordance with [25]). The processes in the boundary layers of MF 2, as explained in 5.2.4, are true, as well, to a large extent for MF 5 (amassing of boundary layer material in the region of the wing tip).

For information regarding the basic effect of taper ratio parameter, please refer to Chapter 5.6.2.

## 5.6 Summary of results on the effect of layout parameter on separation behavior

The following chapter reviews the basic effect of sweep and taper ratio parameters on separation behavior, based on individual results discussed and explained in 5.1 to 5.5. In Chapter 5.6.3, the influence of the flow field's three-dimensionality is discussed and differences of two-dimensional flow are explained.

### 5.6.1 Effect of sweep on separation behavior

By comparing measuring results of wings MF 1 ( $\varphi = 0^\circ$ ), MF 2 ( $\varphi = 30^\circ$ ), and MF 3 ( $\varphi = 45^\circ$ ) it is possible to formulate a /42 statement on the effect of sweep on separation behavior. It is already clear from comparing  $C_A$ - $\alpha$ -curves from the power measurements (Figure 37) that the separation process takes place ever more gradually with increasing sweep (that is, the separation process, on the one hand, extends over a larger

angle of attack region, while on the other it shows a diminishing tendency toward irregular lift alterations).

An increase in sweep, as already mentioned in 5.2 and 5.3, causes two main conditions for the initiation of the separation process:

- a) Span lift maximum (in the case of unseparated flow) moves with increasing sweep from the wing's mid-span section toward the wing tip (Figure 38). This is caused by a decrease of local, effective angle of attack in the wing's mid-span section and an increase of effective angle of attack in the wing's outer region, and is the result of the separation of supporting and free vortices in density direction in the case of the arrowhead wing. For this reason, separation with increasing sweep begins closer and closer to the outer wing.
- b) Added to the effect in a) is the boundary level effect. As sweep increases, boundary material is transported in greater amounts from the wing's mid-span section to the wing tip. This amassing of boundary layer promotes the separation process, particularly because cross-flow occurs most markedly in the rear portion of the wing, in that the boundary layer is already destabilized by the pressure increase in the direction of the trailing edge.

Comparative application of local  $\alpha_{C_{A_{MAX}}}$  values over the 43 span provides a good source of information on the course of separation (Figure 39). The increasing tendency of the curve pattern indicates that the airfoil must traverse an increasing angle of attack region in order to be completely separated. With this, Figure 39 verifies separation behavior derived from power measurements.

The continued path of separation is determined by the roll-up of the separated vortex sheet and the additional velocities induced by this. These velocities may be verified in the nonlinear effects of the  $c_A$ - $\alpha$ -curves.

If, by comparison, we apply  $c_{A_{max}}$  over  $\eta$  and compare it to the profile  $C_{A_{max}}$  in accordance with [25], we obtain a statement on the effect of the flow field's three-dimensionality and on the intensity of non-linear effects which are dependent on sweep (Figure 40). As sweep increases, so, too, does the influence of the vortex sheet on the local lift characteristic. That this influence is not limited to large sweep, may be seen, for example, from the  $c_A$ - $\alpha$ -curves of the MF 2, reproduced in Figure 20 (as already explained in 5.2).

With the considerations in 5.3.4, the flow field of a swept wing is a pre-stage of the flow field of a slim delta wing with leading edge separation. Apparently, a separating line equally swept by wing sweep is decisive, and not the location of this separating line on the airfoil.

This is supported by the fact that, as in the case of /44 MF 3, local  $c_A$ - $\alpha$ -patterns were measured which are similar to the  $C_A$ - $\alpha$ -pattern of a slim delta wing. In addition to this, pressure distributions have similar patterns, too. Figure 41 compares the pressure distribution of a slim delta wing according to [27] with a pressure distribution on the MF 3. The qualitative agreement may be considered good. It may be assumed that the similar pressure distributions result from similar flow fields.

In spite of the varied flow fields forming on the three wings, the  $C_{A_{max}}$  values lie only a few percentage points apart (see also Figure 37). It is absolutely necessary to be aware of the fact that with increasing sweep at  $\alpha_{C_{A_{max}}}$ , constantly larger areas are already separated on the airfoil, and, for this reason, the "usable"  $C_{A_{max}}$  and/or  $\alpha_{C_{A_{max}}}$  (the condition by which the

flow only just completely attaches) decreases with  $\varphi$  (this can also be seen from Figure 37).

### 5.6.2 Effect of taper ratio on separation behavior

The parameter of taper ratio can be investigated using wings MF 2 ( $\lambda = 1.0$ ), MF 4 ( $\lambda = 0.5$ ), and MF 5 ( $\lambda = 0.25$ ). As the results show, the effect of the boundary layer hardly alters as the result of the given constant sweep of the quarter chord line. All three wings exhibit typical cross-flow to the wing tip determined by sweep.

The span  $c_A$  distribution is more markedly affected by /45 a change in taper ratio. Increasing taper ratio has an effect similar to enlarging sweep: span maximum of the lift factor moves outward and increases radically. This means that the  $c_A$  load in the outer wing region increases markedly (Figure 42).

From the application of  $\alpha_{C_{A_{MAX}}}$  over  $\eta$  we recognize that, as expected, the separation process in the outer wing region begins earlier with increasing taper ratio, that is, at smaller angles of attack (Figure 43). At the same time, it becomes clear that the separation process stretches over a larger angle of attack region. The  $c_A$ -distribution is also responsible for this to a certain extent, since the  $c_A$  load in the wing's mid-span section decreases together with the increase of the  $c_A$  load on the wing tip (for  $\lambda \rightarrow 0$ ). The direction of transport inside the boundary layer also supports the stabilizing or destabilizing affect of the  $c_A$ -distribution, according to its position on the wing.

If we compare the pattern of the wall flow line for a constant angle of attack, where no separation has yet occurred on any of the wings (for example,  $\alpha = 8^\circ$ ), then we see that the cross-flow intensity (measured over the curvature of the wall flow line in the colored pictures) decreases with increasing

taper ratio (Figure 44). The decrease of taper ratio (and with it, also, outer density), however, has a smaller trailing edge sweep as a result. This causes the pressure gradient beginning at a diagonal to the flow direction to decrease, and, with it, so does the cross-flow in the boundary layer (Figure 45). This effect explains how the maximum lift factor in the inner region of the wing decreases with the taper ratio (Figure 46).

### 5.6.3 Effect of the flow field's three-dimensionality on separation behavior

With the results cited here, three main types of separation can be defined:

- a) If the separated vortex sheet is fed from both sides of the separating line with circulation from attaching flow, then this type of separation has no dead water area on the airfoil as a result. This type is known, for example, as leading edge separation on slim delta wings and occurs, likewise, in the form of a tip vortex on the side edges of all the airfoils investigated in this study. This tip vortex has a strong, albeit locally limited induction effect, which can be clearly recognized from pressure distributions. Furthermore, the measuring results from MF 3 particularly encourage the interpretation that the vortex sheet rolls up on the airfoil in a similar fashion (see Chapter 5.3.4 regarding this). The intensity of these processes, however, as could be shown, is connected to the wing's sweep, and with it, also, to the sweep of the separating line.
  
- b) The second form of separation can be compared, at least partially, with separation characteristics of two-dimensional profile. Here, flow separates on two separating lines, of which one lies mostly in the

trailing edge. A dead water region forms and is surrounded by the two separated vortex sheets. This type of separation possesses a displacement effect and, for this reason, is comparable to two-dimensional dead water areas /47. These vortex sheets do not have the character of an unstable position displaying velocity irregularities, but rather a shearing layer character. In spite of basically strongly turbulent structure inside this dead water, main flow directions are defined by the velocity and pressure gradients which are present in span and depth. For completely separated flow, a pressure pattern occurs here, for which the dead water pressure is not constant in span nor, to a limited extent, in depth.

- c) Furthermore, there is a mixed form of types a) and b). In the separation area between attaching and separated flow, an increase in cross velocities is caused by span circulation gradients which develop. The separated portion of the vortex sheet then tends to roll up over the attaching portion. This process was designated with the name "part-span-vortex-sheet" by Kuechemann [16]. This flow form is found in all five airfoils, although the inducing effect of the rolling up process is markedly varied.

## 6. Summary

Separation behavior on two-dimensional profiles is dependent on the parameters of profile type and Reynolds-number (for incompressible flow, that is,  $M < 0.2$ ). As the results cited here show, the parameters of wing layout and span lift /48 distribution and/or  $C_A$ -distribution (for swept wings) must be added for three-dimensional airfoils. In the study presented here, I have attempted to determine the effect of the last two parameters using wind tunnel measurements on a model system

consisting of five airfoils of equal aspect ratio, but of different sweep and taper ratio. The most important results may be summarized as follows:

- The separation effect on wings of moderate aspect ratio is three-dimensional. It is not possible to predict the separation process by observing the airfoil divided into even span sections onto which separation characteristics of two-dimensional profile are brought to bear.
- The areas separated in the airfoil, as far as we are dealing with the type of separation described in 5.6.3 b), are to be considered to be three-dimensional in spite of the dead water character.
- According to 5.6.3 a), the rolling up of separated vortex sheets increases in intensity and induction effect with sweep and has marked nonlinearity in local  $C_A-\alpha$  pattern as a result.
- Boundary layer material is transported at a diagonal to the flow direction by pressure gradients present on the airfoil. Removal of boundary material basically has a stabilizing effect on the wing boundary layer; build up of boundary material has a destabilizing effect (and with it, one favorable to separation).
- The separation process begins earlier with increasing 49 taper ratio (that is, at smaller  $\alpha$ ). At the same time, the angle of attack region increases until it reaches the completely separated condition.
- With both increasing taper ratio and increasing sweep, angle of attack difference gets larger between the angle of attack for which flow on the wing is still completely attached and the angle of attack of the maximum lift factor.

## REFERENCES

- 1 Kuechemann, D., "Types of Flow over Swept Wings with Special References to Free Boundaries on Vortex Sheets," J. Roy. Aero Soc., 683, 1953.
- 2 Kuechemann, D., "Boundary Layers on Swept Wings: Their Effects and their Measurement," RAE TN-Aero-2370, 1955.
- 3 Gault, D. E., "A Correlation of Low-Speed, Airfoil Section Stalling Characteristics with Reynolds Number and Airfoil Geometry," NACA TN-3963, 1957.
- 4 Seetharam, H. C., and W. H. Wentz, "Studies of Flow Separation and Stalling on One- and Two-Element Airfoils at Low Speed," SAE 770442, 1977.
- 5 Young, H. W., and D. R. Hoad, "Comparison of Two Flow Surveys above Stalled Wings," AIAA-79-0332, 1979.
- 6 Hall, M.G., "Scale Effects on Flow over Swept Wings," RAE TR-71043, 1971.
- 7 Maskell, E. C., "Flow Separation in Three Dimensions," RAE Rep. Aero 2565, 1955.
- 8 Peake, D. J., and M. Tobak, "Three-Dimensional Separation and Reattachment," NASA TM-84221, 1982.
- 9 Tobak, M., and D. J. Peake, "Topology of Two-Dimensional and Three-Dimensional Separated Flows," AIAA-79-1480, 1979.
- 10 Pinkerton, R. M., "Calculated and Measured Pressure Distributions over the Mid-Span Section of the NACA 4412 Airfoil," NACA TR-563, 1936.
- 11 Werle, H., "Separation Types on Arrowhead Wings," Rech. Aerosp. No. 1980-2, pp. 86-108.
- 12 Schmitt, V., and F. Manie, "Subsonic and Transsonic Flow on a Variable Arrowhead Wing," Rech. Aerosp. No. 1979-4, pp. 219-237.
- 13 Kohler, M., "Regarding Flow Processes on Oblique and Stalled Airfoils during Parallel Movement and Rotation," Luftfahrtforschung Band 16, Lfg. 4, 1939.
- 14 Jacob, K., "Computation of the Flow Around Wings with Rear Separation," DFVLR-FB-82-22, 1982.
- 15 Winkelmann, A. E., H. T. Ngo, and R. C. Deseife, "Some Observations of Separated Flow on Finite Wings," AIAA-82-0346, 1982.
- 16 Winkelmann, A. E., "An Experimental Study of Separated Flow on a Finite Wing," AIAA-81-1882, 1981.
- 17 Lip, L. P., and G. L. Shubert, "Pressure Distribution on a 1-by 3-Meter Semispan Wing at Sweep Angles from 0° to 40° in Subsonic Flow," NASA TN D-8307, 1976.
- 18 Hummel, D., "Regarding Flow Around Sharp-Edged Slim Delta Wings at Large Angles of Attack," ZFW 15, Heft 10, 1967.
- 19 Rettig, K., "The 3-Meter Low-Speed Wind Tunnel at the Institute for Flight Technology of the Technical University Darmstadt," ZFW 23, Heft 10, 1975.
- 20 Keil, J., and M. Quade, "Description of the Data Processing Equipment on the 3-Meter Low-Speed Wind Tunnel," IFD 4/79, Institute for Flight Technology, TH Darmstadt.

- 21 Keil, J., "Experimental Investigations on Airfoils of Different Geometries in the Region of High Angles of Attack," Measuring Report on Research Projects Ha 514/57, Institute for Aerodynamics and Measuring Technology, TH Darmstadt, A 5/1984, Part 2.
- 22 Schlichting, H., and E. Truckenbrodt, Aerodynamik des Flugzeugs, Bd. I + II (Aerodynamics of Aircrafts, Volumes I + II), Springer Verlag, Berlin, 1967.
- 23 Hornung, G., "Regarding the Topological Structure of Separated Flow with Three-Dimensional Parameter Conditions," Report at DGLR-Symp. "Flows with Separation," Stuttgart, Nov. 23-25, 1981.
- 24 Keil, J., "Experimental Investigations on Airfoils of Different Geometries in the Region of High Angles of Attack," Report at DGLR-Symp. "Flows with Separation," Stuttgart, Nov. 23-25, 1981.
- 25 Abbot, I. H., and A. E. von Doenhoff, Theory of Wing Sections, Dover Pub., New York, 1959.
- 26 Kraemer, K., "Regarding the Effect of Trip Wires on Boundary Layer Transition," ZFW 9, Heft 1, 1961.
- 27 Wick, B. H., Chordwise and Spanwise Loadings Measured at Low Speed on a Triangular Wing having an Aspect Ratio of Two and a NACA 0012 Airfoil Section," NACA TN-1650, 1948.

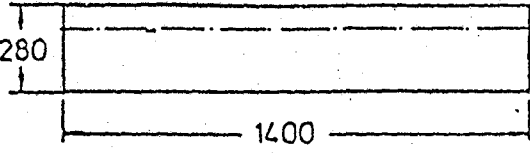
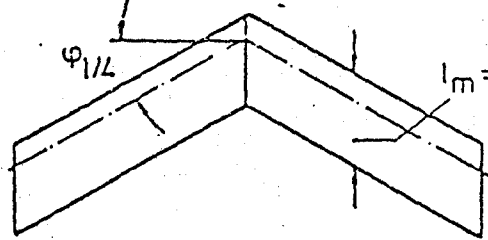
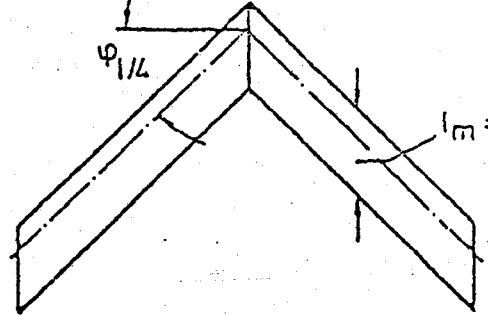
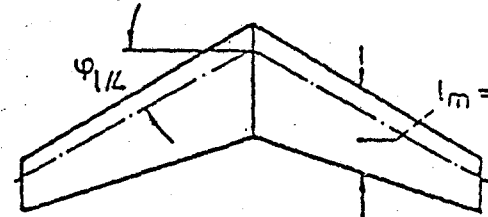
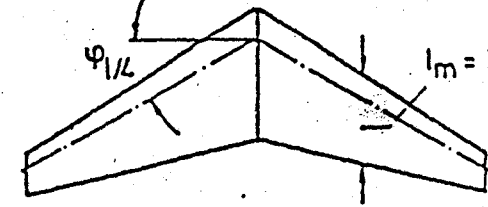
<p style="text-align: center;"><u>MF1</u></p> $\Lambda = 5$ $\varphi_{1/2} = 0^\circ$ $\lambda = 1$	
<p style="text-align: center;"><u>MF2</u></p> $\Lambda = 5$ $\varphi_{1/2} = 30^\circ$ $\lambda = 1$	
<p style="text-align: center;"><u>MF3</u></p> $\Lambda = 5$ $\varphi_{1/2} = 45^\circ$ $\lambda = 1$	
<p style="text-align: center;"><u>MF4</u></p> $\Lambda = 5$ $\varphi_{1/2} = 30^\circ$ $\lambda = 0.5$	
<p style="text-align: center;"><u>MF5</u></p> $\Lambda = 5$ $\varphi_{1/2} = 30^\circ$ $\lambda = 0.25$	

Figure 1 Layout Parameter of Wings MF 1 to MF 5

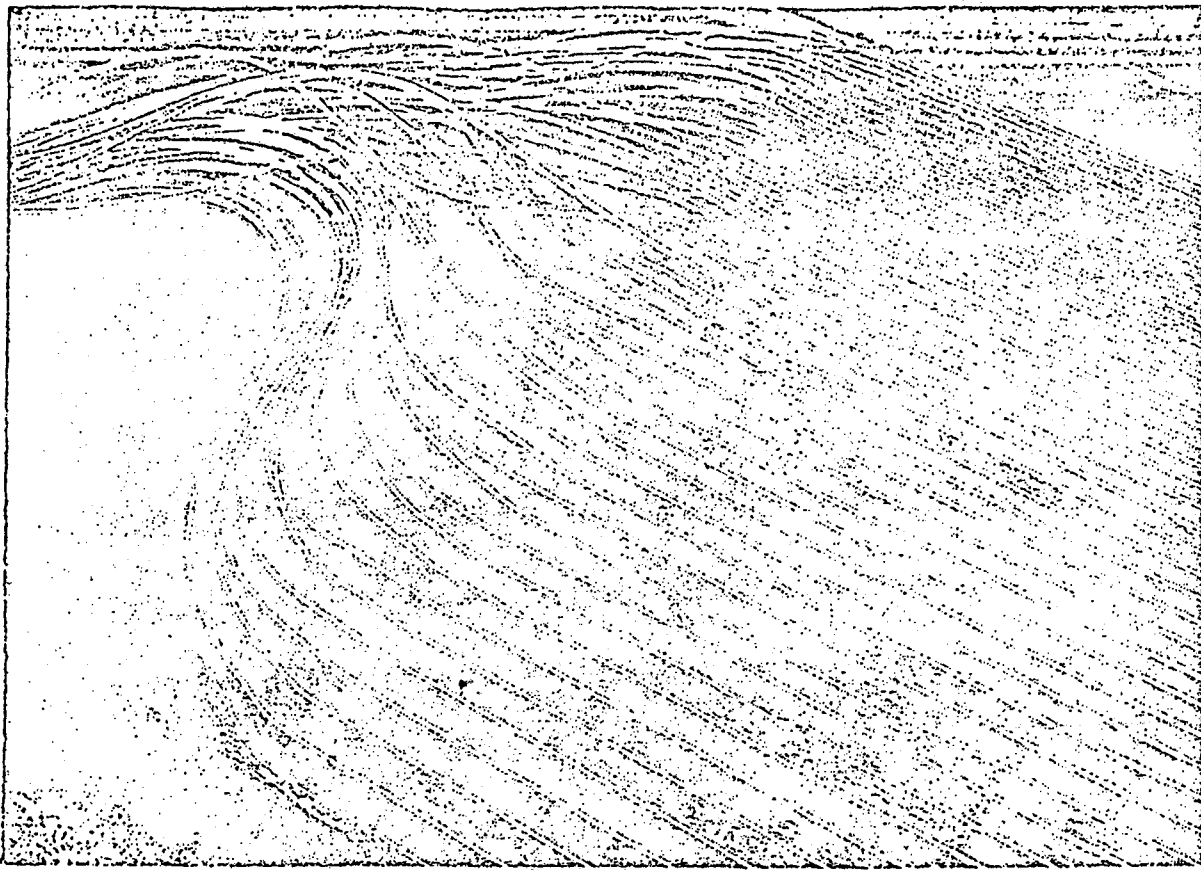


Figure 2 Arrangement of Pressure Measuring Tubes on MF 1

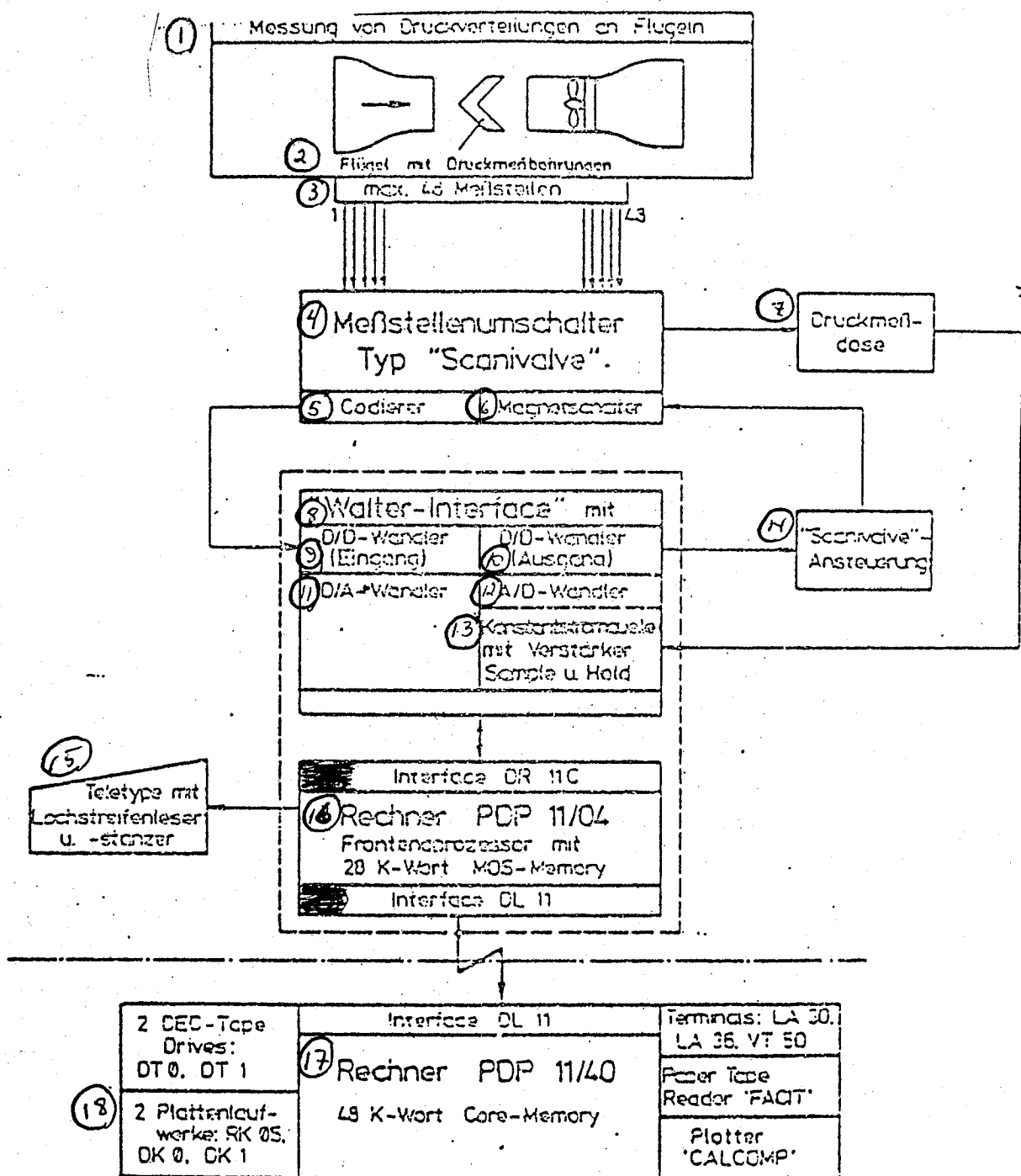
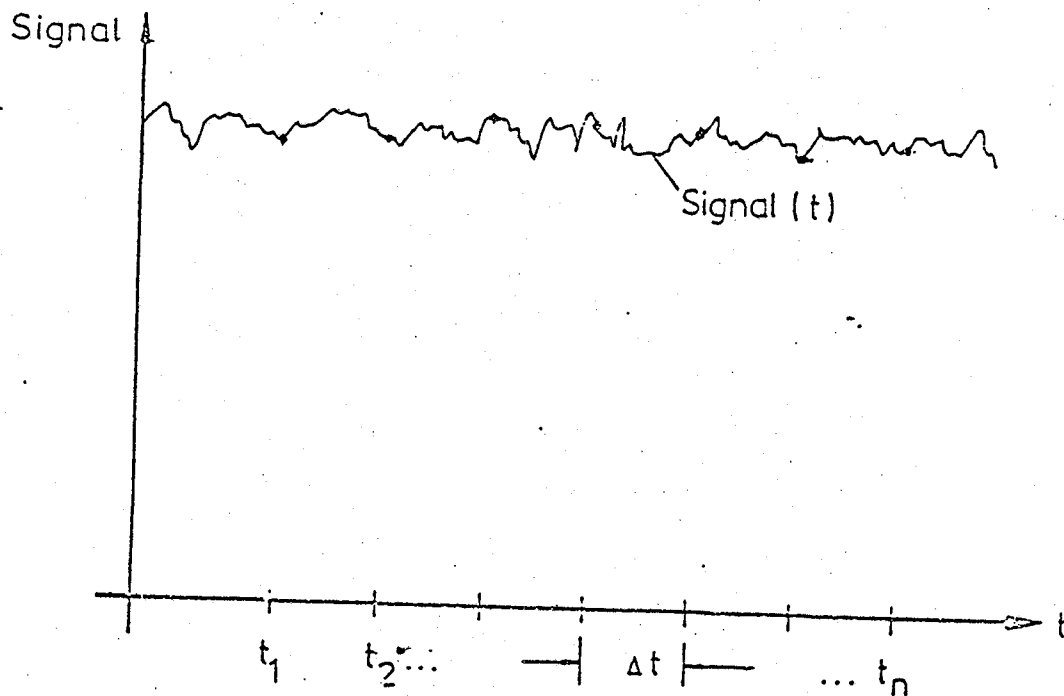


Figure 3 Data Processing on Low-Speed Wind Tunnel

Key: 1) Measurement of Pressure Distribution on Wings  
 2) Wings with Pressure Measuring Borings 3) Max. 48 Measuring Points  
 4) "Scanivalve" Brand Measuring Point Switch 5) Coder 6) Magnetic Switch 7) Pressure Measuring Box  
 8) "Walter Interface" with 9) D/D Converter (Input) 10) D/D Converter (Output)  
 11) D/A Converter 12) A/D Converter 13) Constant Flow Control with Amplifier Sample and Hold  
 14) "Scanivalve" Control 15) Teletype with Tape Reader and Key Punch  
 16) PDP 11/04 Computer, Front-end Processor with 28 K Word and MDS Memory  
 17) PDP 11/40 Computer, 48 K Word and Core Memory 18) 2 Disk Drives



$$1) \text{ Meßwert} = \frac{\sum_{i=1}^n \text{Signal}(t_i)}{n}$$

2) Wobei  $n$  und  $\Delta t$  weitgehend frei wählbar sind.

**Figure 4** Measuring Process to form Average Values using Measuring Signals with Variation Portions  
 Key: 1) Measuring Value 2) Whenever  $n$  and  $\Delta t$  are to a large extent selectable

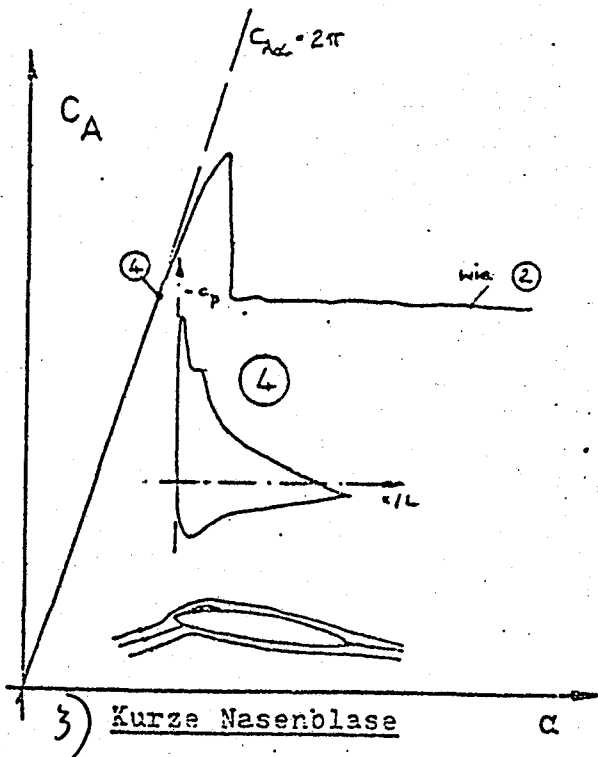
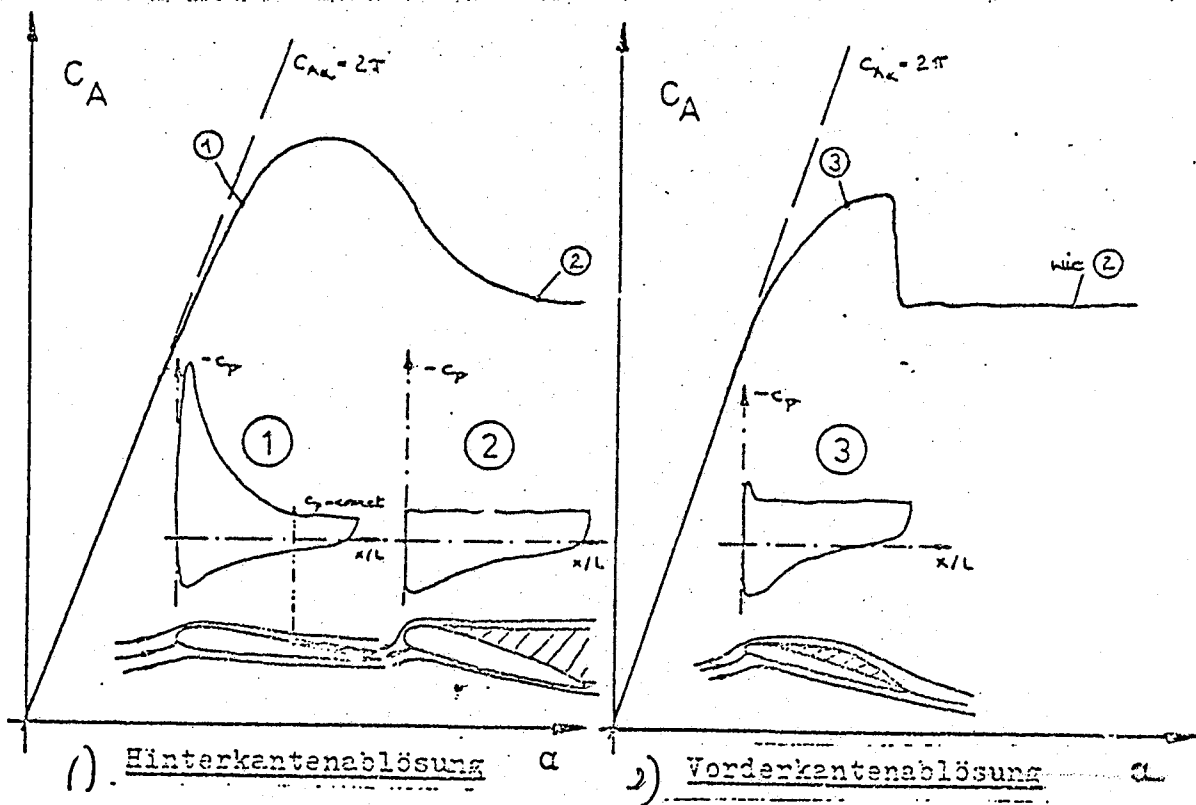
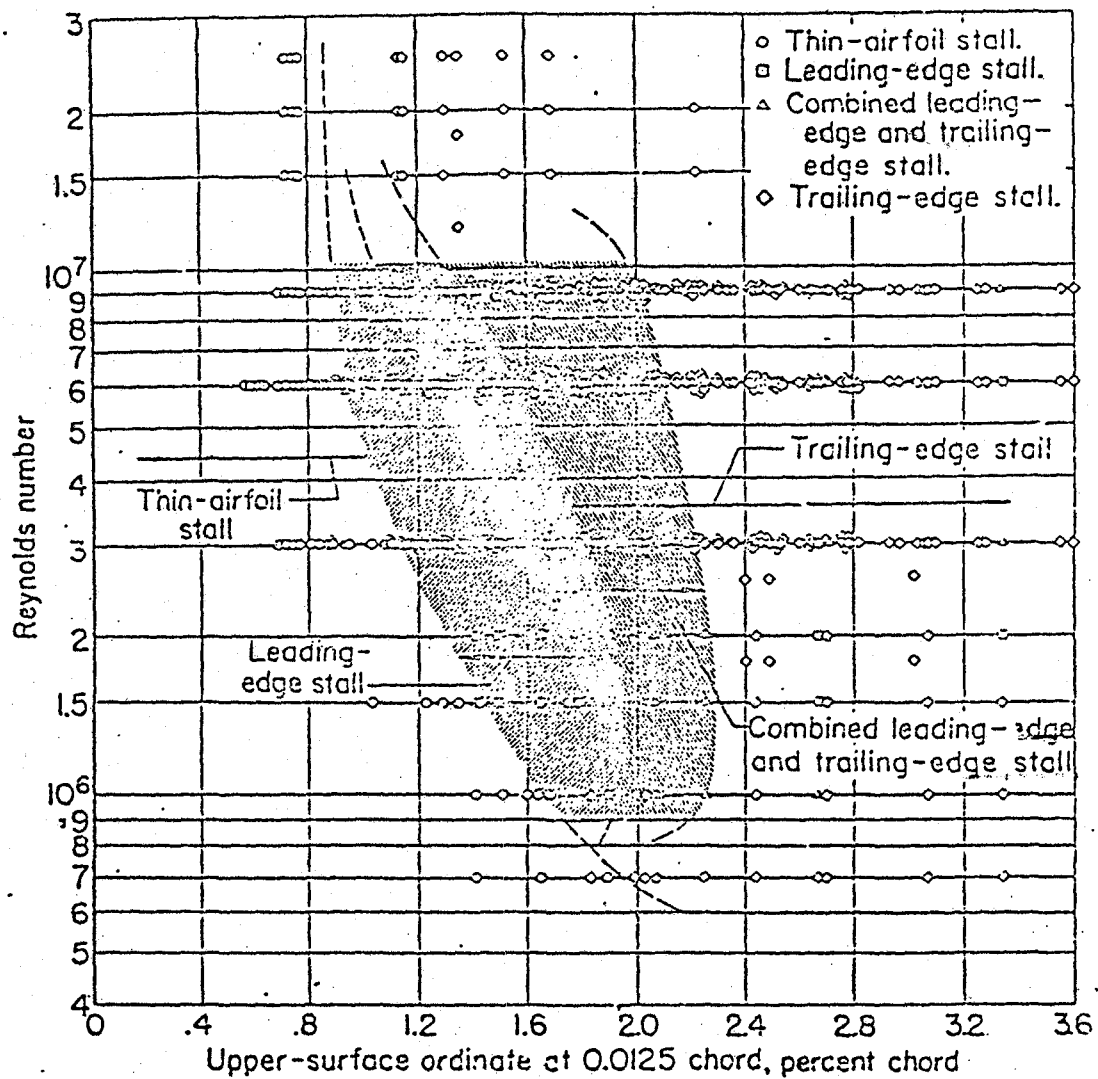


Figure 5 Separation Types at Subsonic Flow Around Profile. Representation of Typical  $C_A$  - Patterns, Pressure

Key: 1) Trailing Edge Separation 2) Leading Edge Separation 3) Short Nose Bubble



The low-speed stalling characteristics of airfoil sections correlated with Reynolds number and the upper-surface ordinates of the airfoil sections at the 0.0125-chord station.

Figure 6 Gault - Diagram according to [3]

M F 1

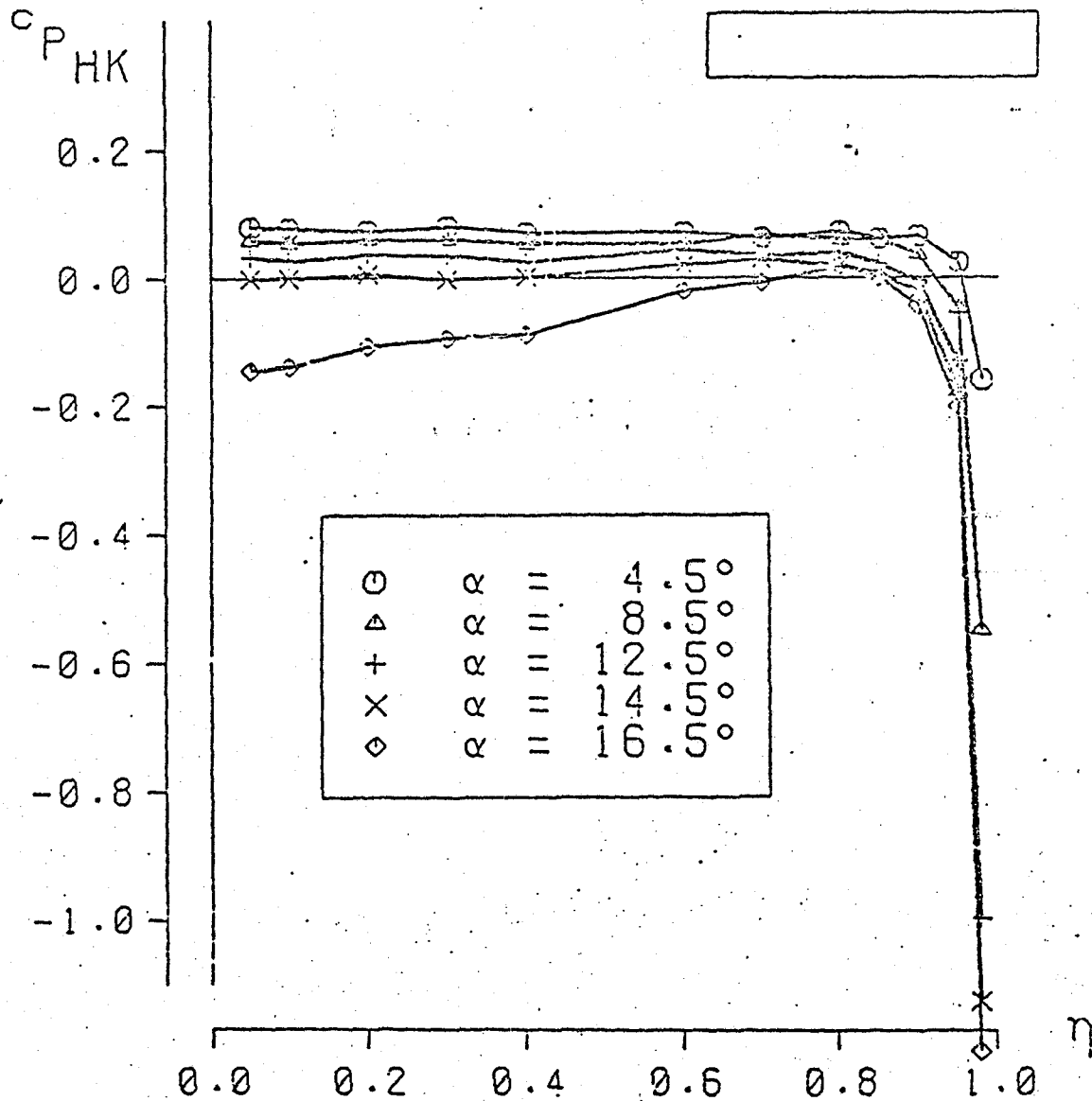


Figure 7 Pattern of the Trailing Edge Pressure Factor  $c_{P_{HK}}$  over the Span as a Function of Angle of Attack

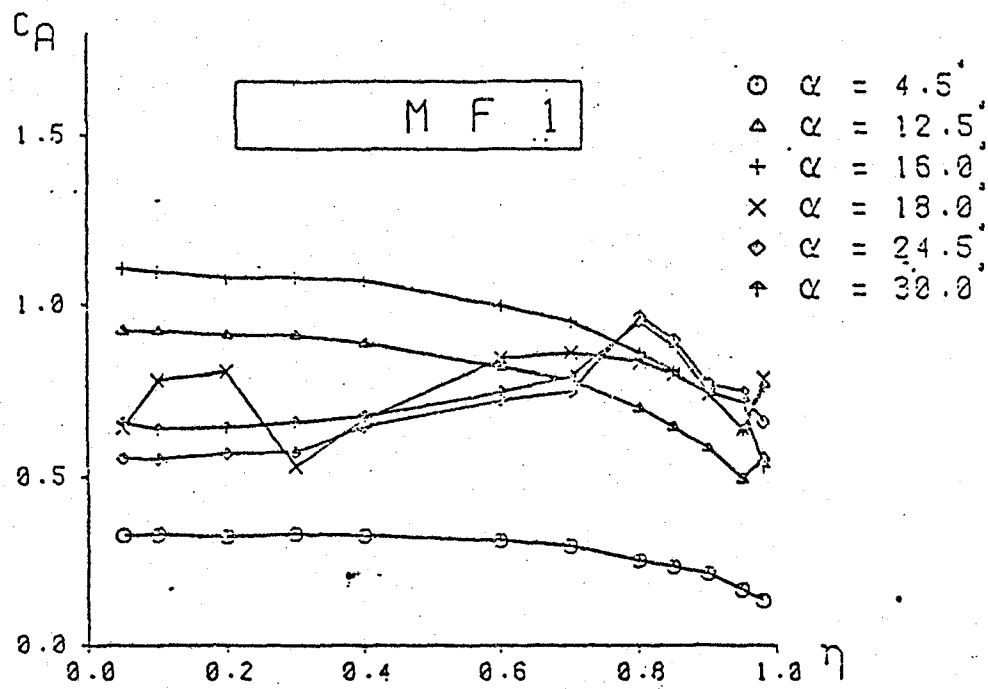


Figure 8 Span Lift Distributions on MF 1

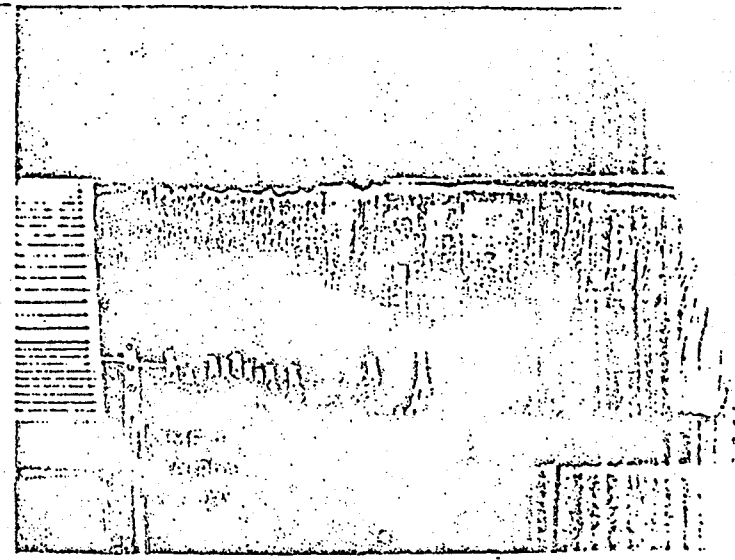


Bild 10

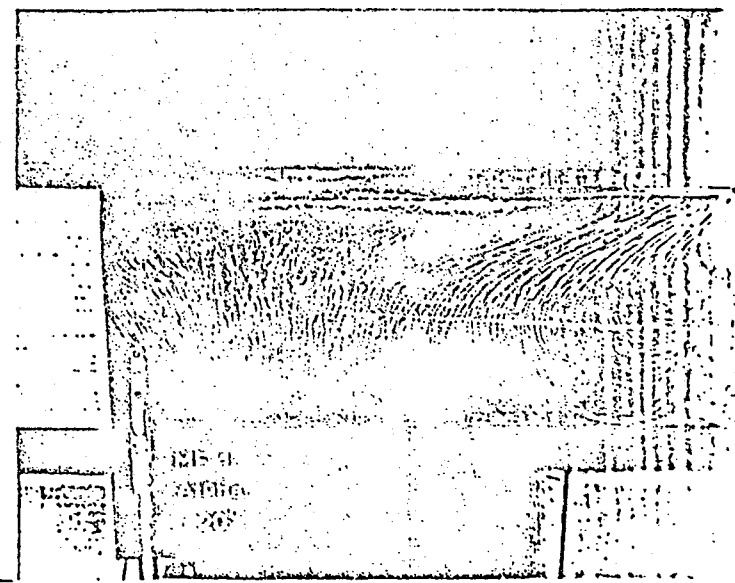


Bild 12

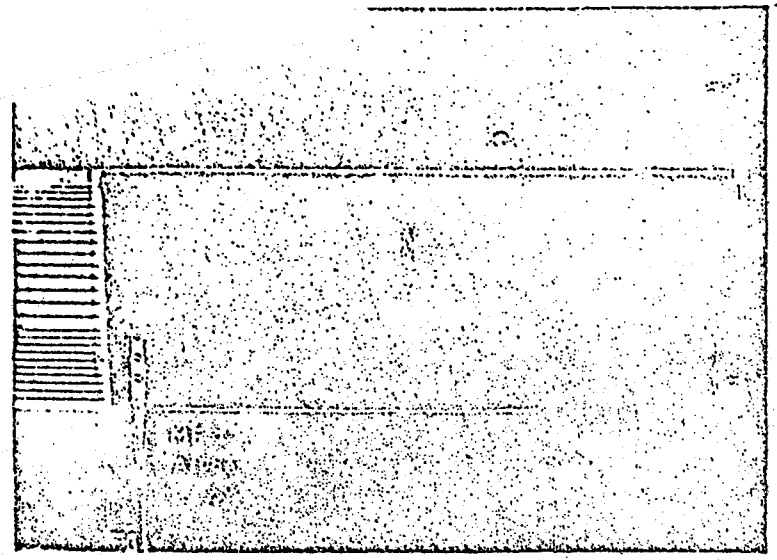


Bild 9

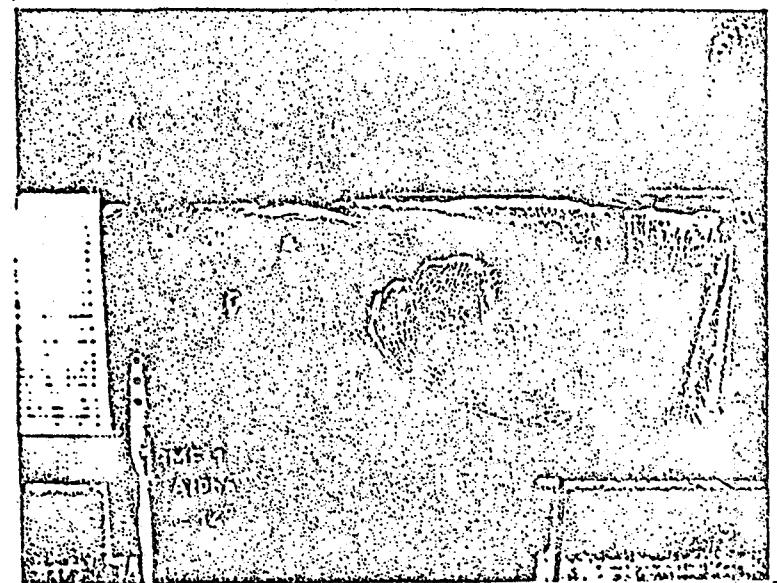


Bild 11

Figures 9 to 12 Representation of Tangential Wall Stress Pattern  
 on the Wing's Upper Side with a Colored Process;  
 Wing MF 1  
 "Bild" = "Figure"

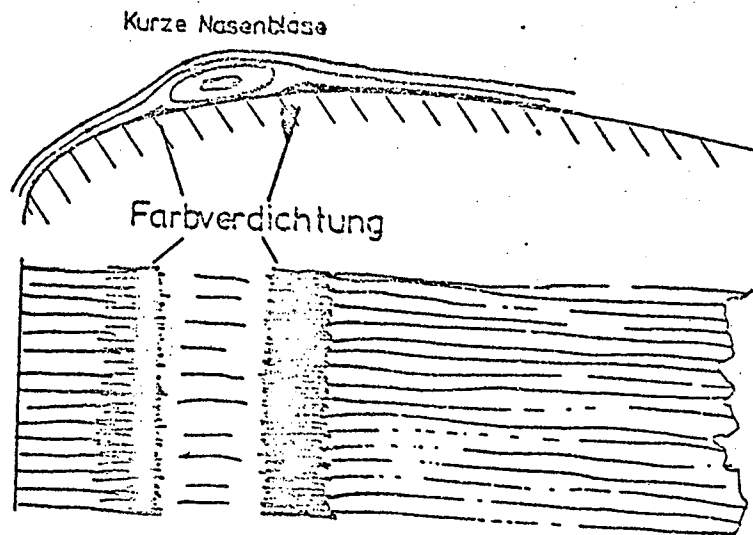
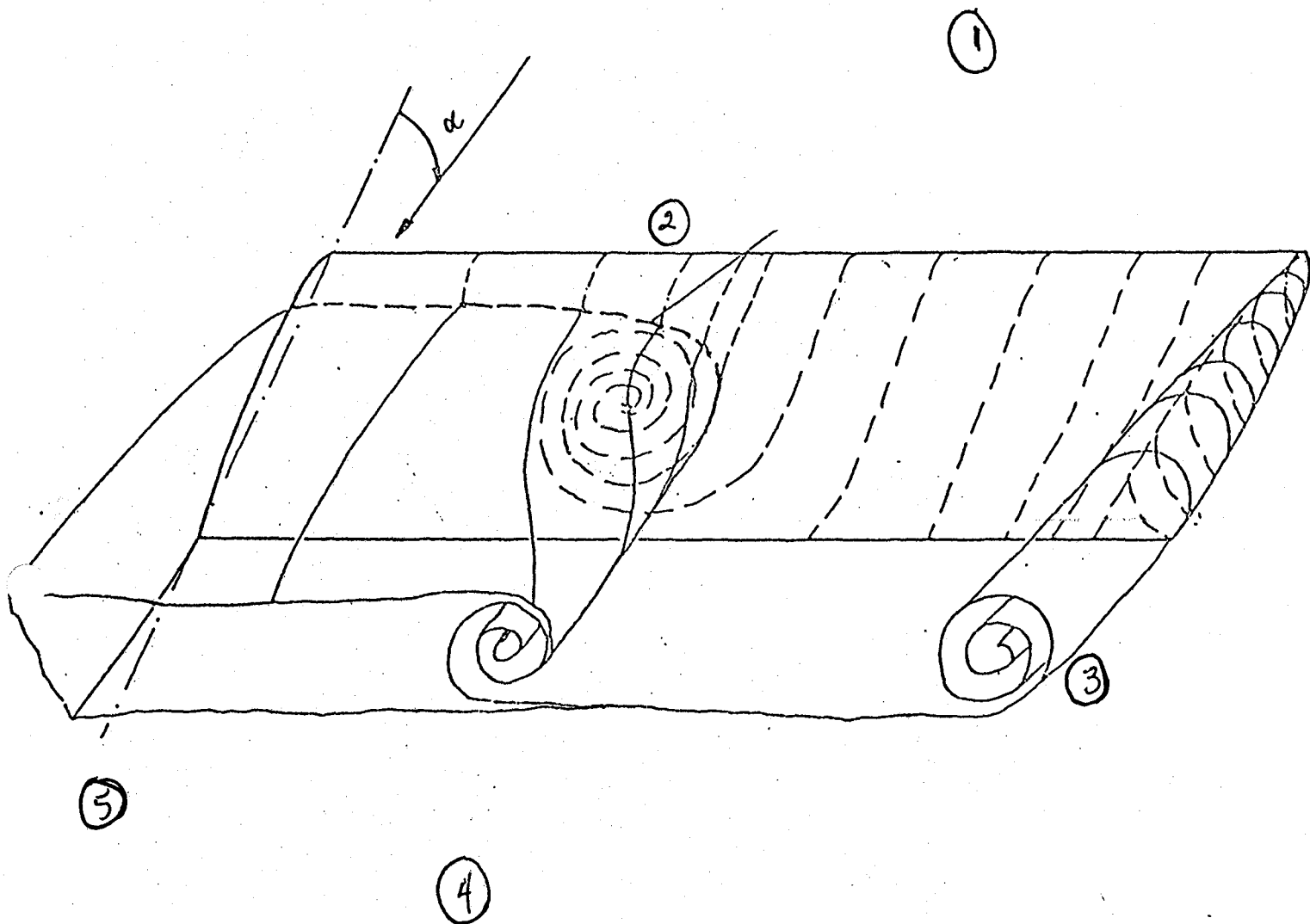


Figure 13 Formation of Color Structure, Caused by a Short Nose Bubble

Key: 1) Short Nose Bubble 2) Color compression



**Figure 14** Flow Model for Partially Separated Flow on MF 1;  $\alpha \approx 18^\circ$

Key: 1) Flow Direction in ----- Vortex Sheet  
 in - - - - - Boundary Layer 2) Separating Line 3)  
 Tip Vortex 4) Rolling up of the Vortex Sheet in the  
 Boundary Area to the Attaching Flow 4) Separated Flow  
 with Dead Water Character

M F 2

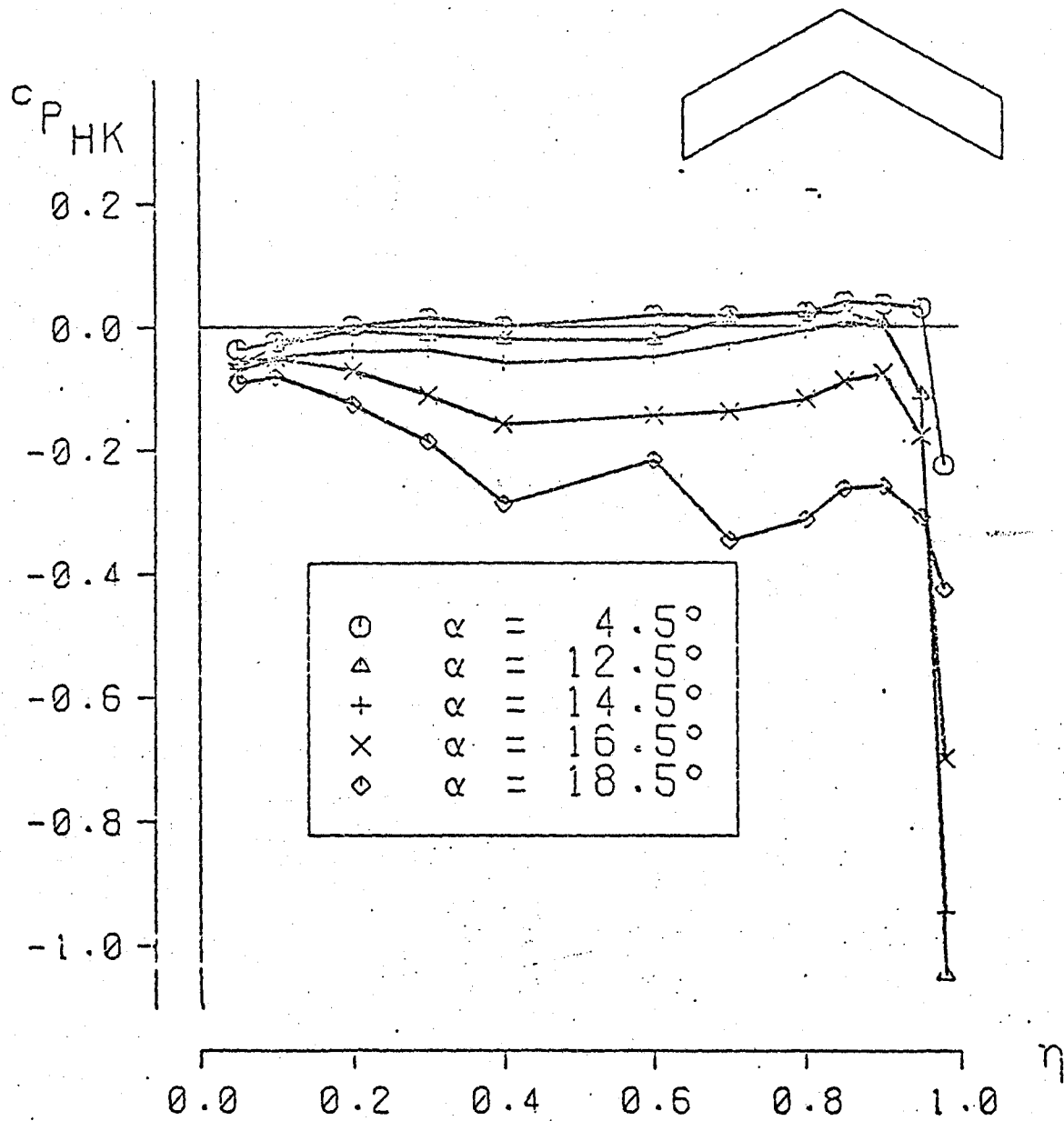


Figure 15 Pattern of the Trailing Edge Pressure Factor  $c_{P_{HK}}$  over the Span as a Function of Angle of Attack

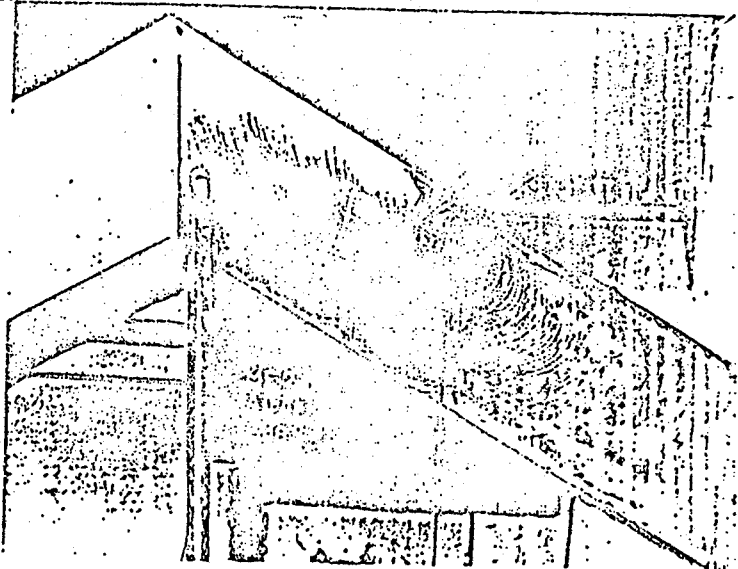


Bild 17

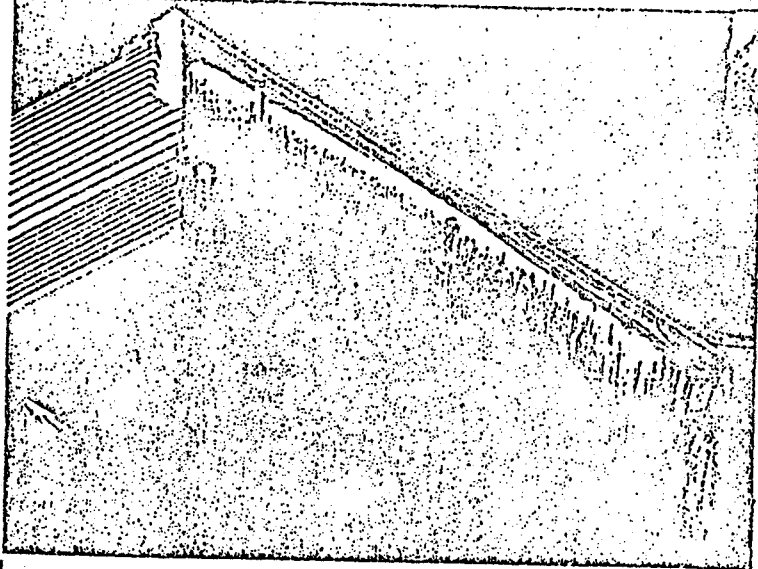


Bild 16

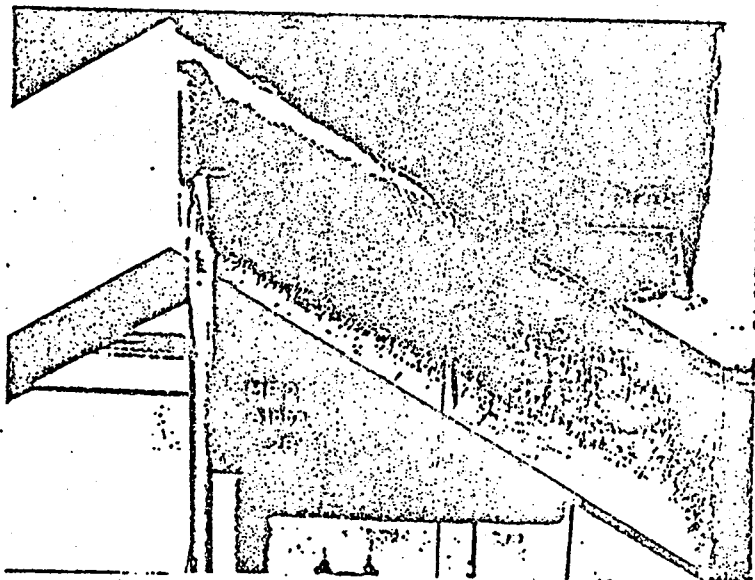
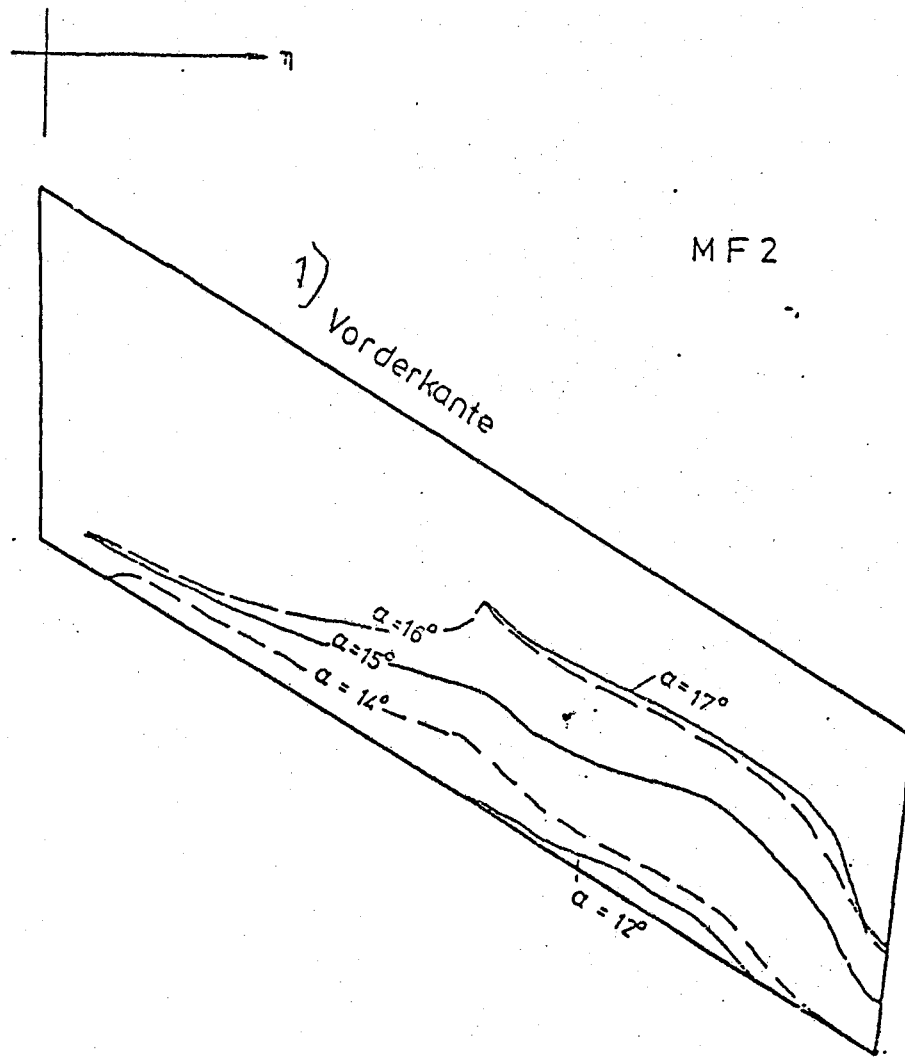


Bild 18

Figures 16 to 18 Representation of Tangential Wall Stress  
Pattern on the Wing's Upper Side with a Colored  
Process; Wing MF 2  
"Bild" = "Figure"



**Figure 19** Separating Flow Line Pattern on MF 2 as a Function of Angle of Attack (Taken from Colored Pictures)  
 Key: 1) Leading Edge

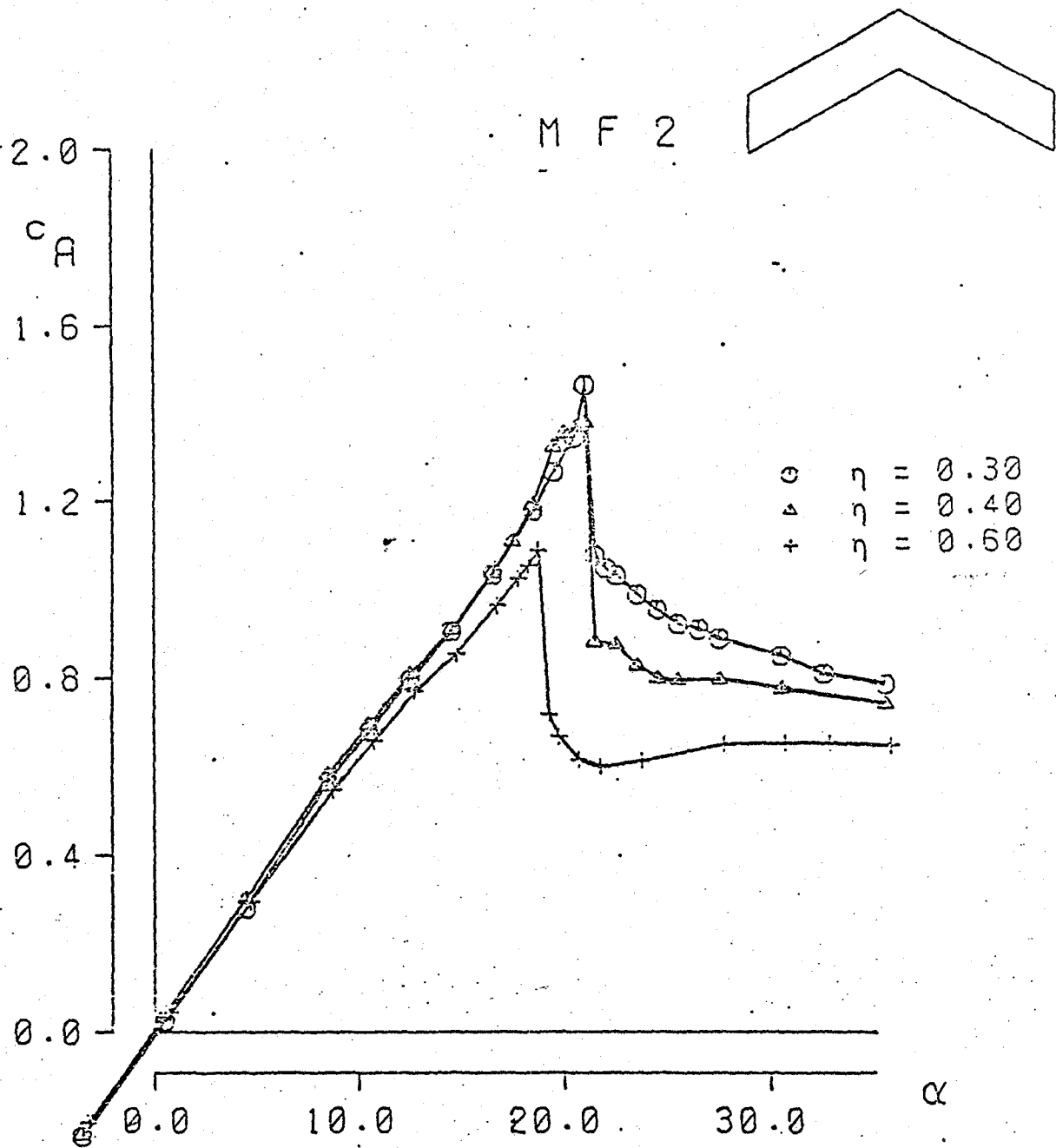


Figure 20 Function of Lift Factor over Angle of Attack for Different Span Measuring Sections

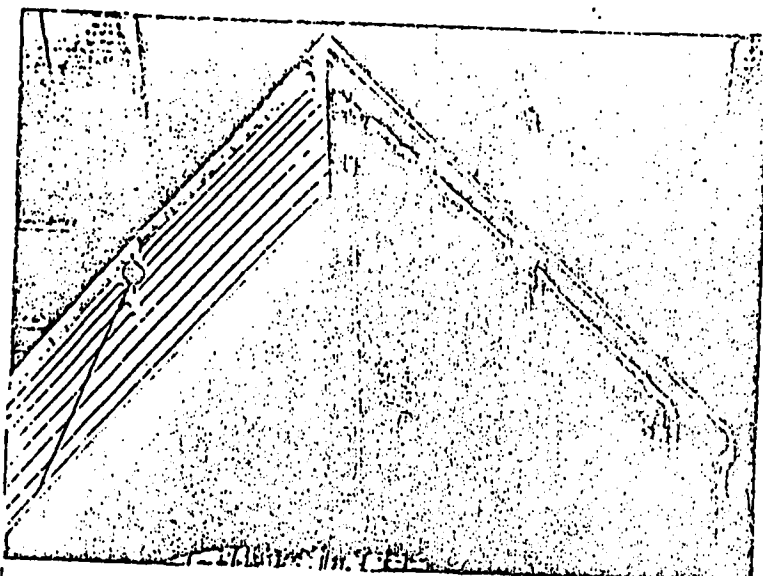


Bild 21

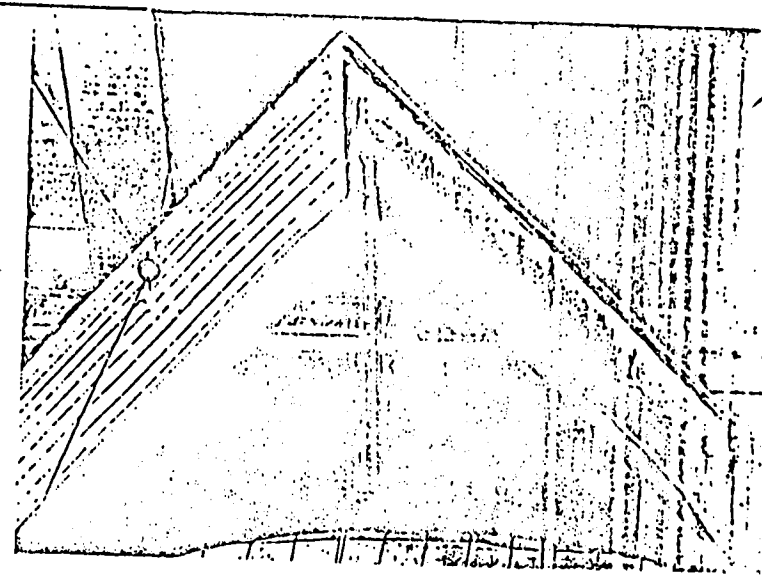


Bild 22 ;  $\alpha = 10^\circ$

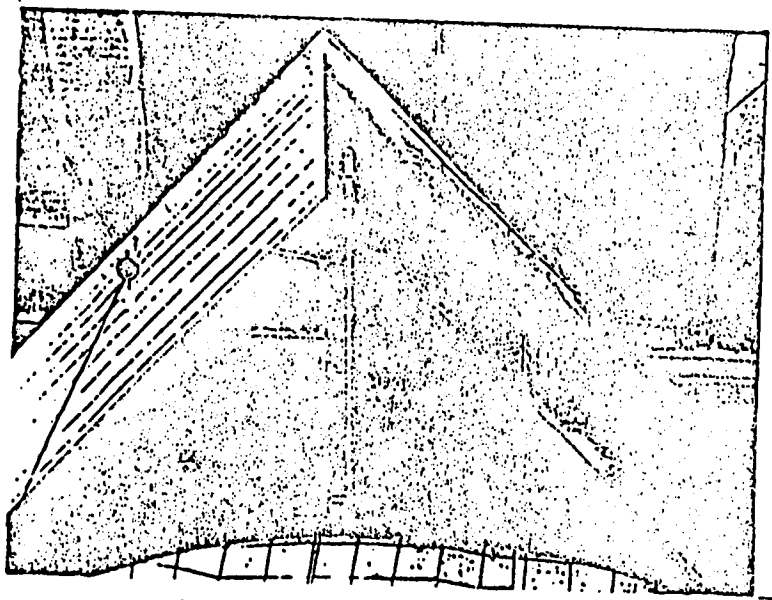


Bild 23

Figures 21 to 23 Representation of Tangential Wall Stress  
 Pattern on the Wing's Upper Side with a Colored  
 Process; Wing MF 3  
 "Bild" = "Figure"

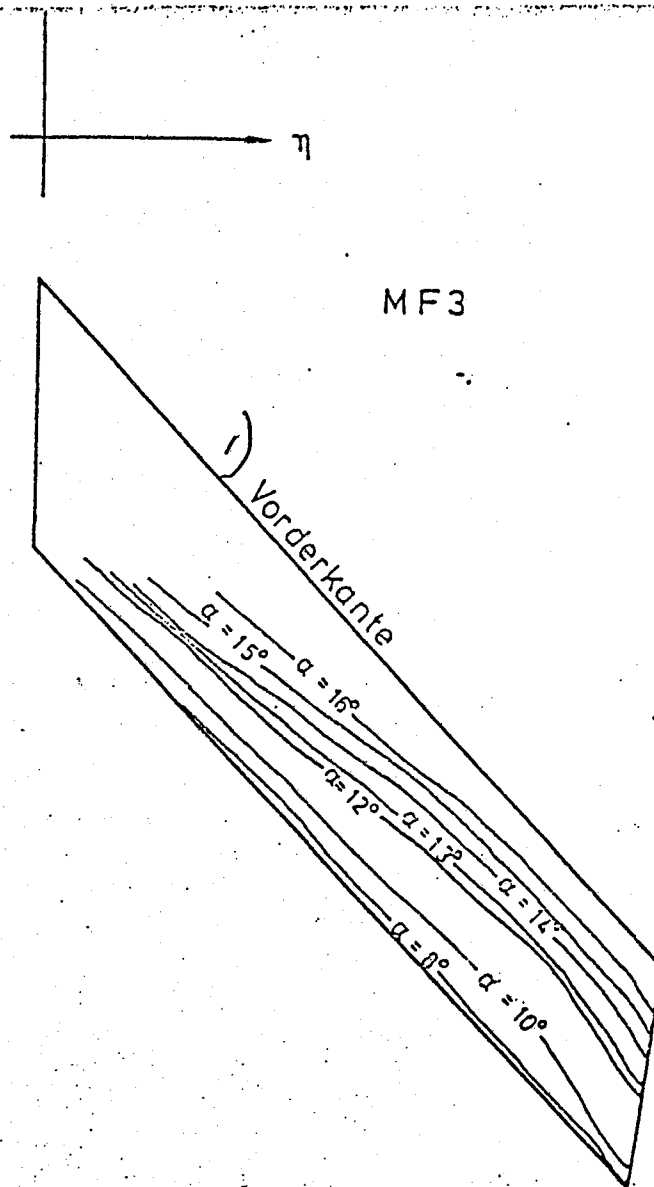


Figure 24 Separating Flow Line Pattern on MF 3 Dependent on Angle of Attack (Taken from Colored Pictures)  
 Key: 1) Leading Edge

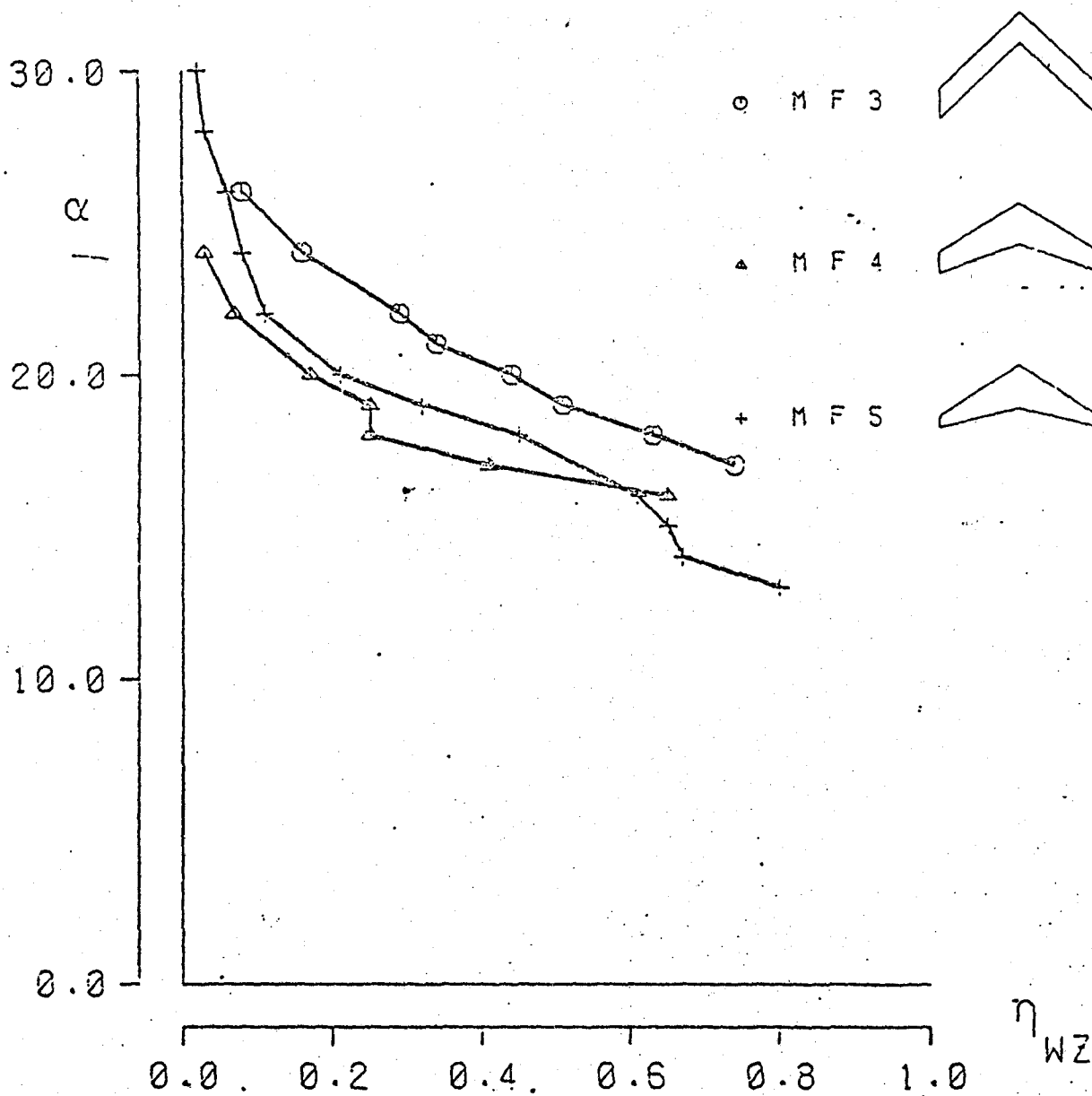


Figure 25 Location of Vortex Center (Taken from Colored Pictures) in Dependence on Angle of Attack

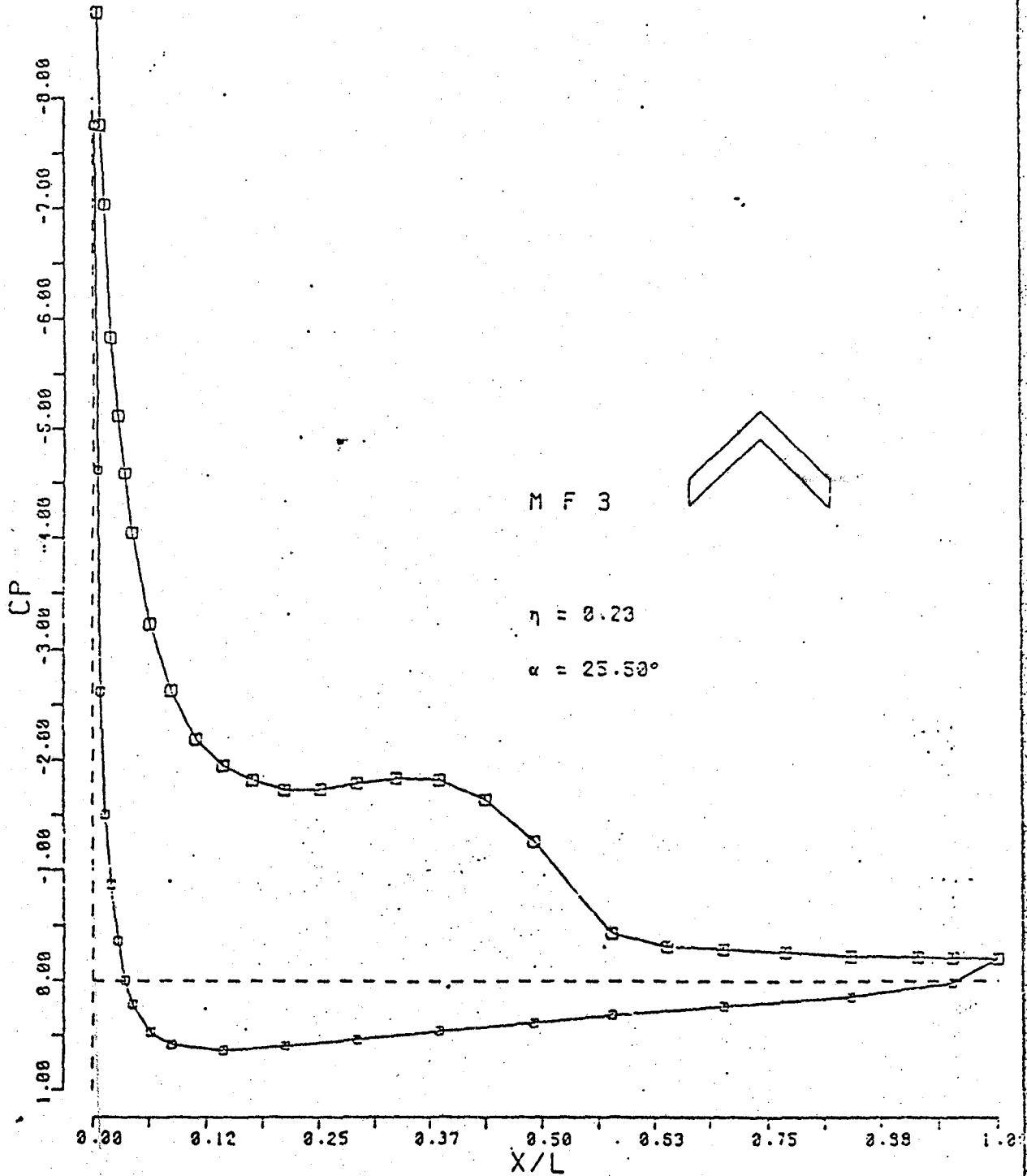


Figure 26 Pressure Distribution on MF 3

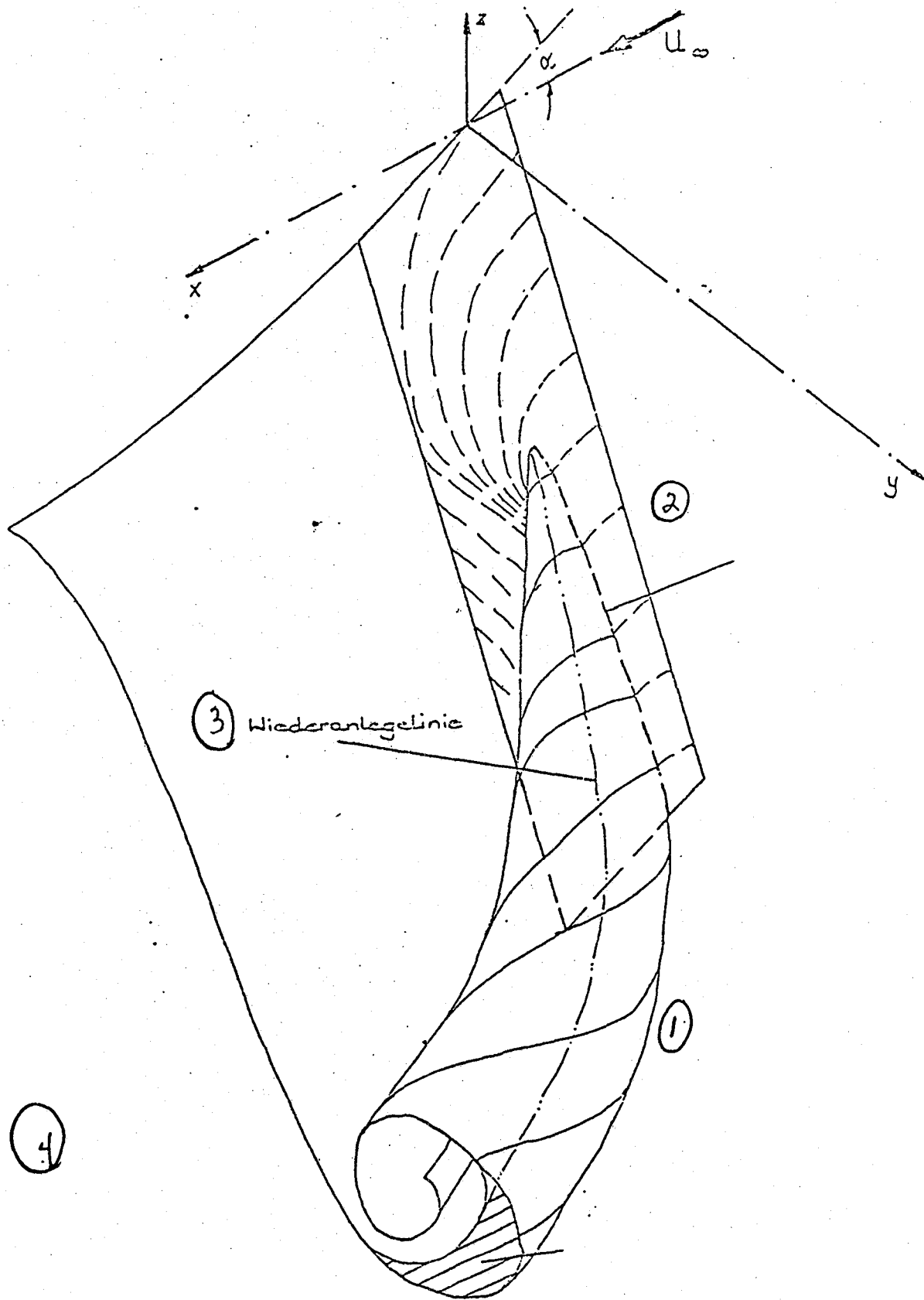
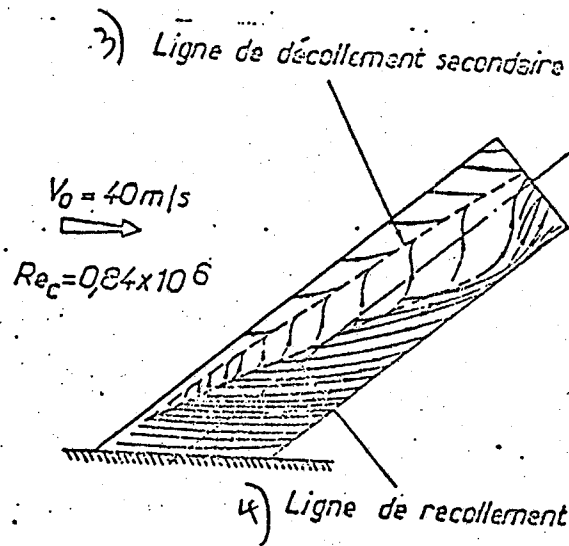
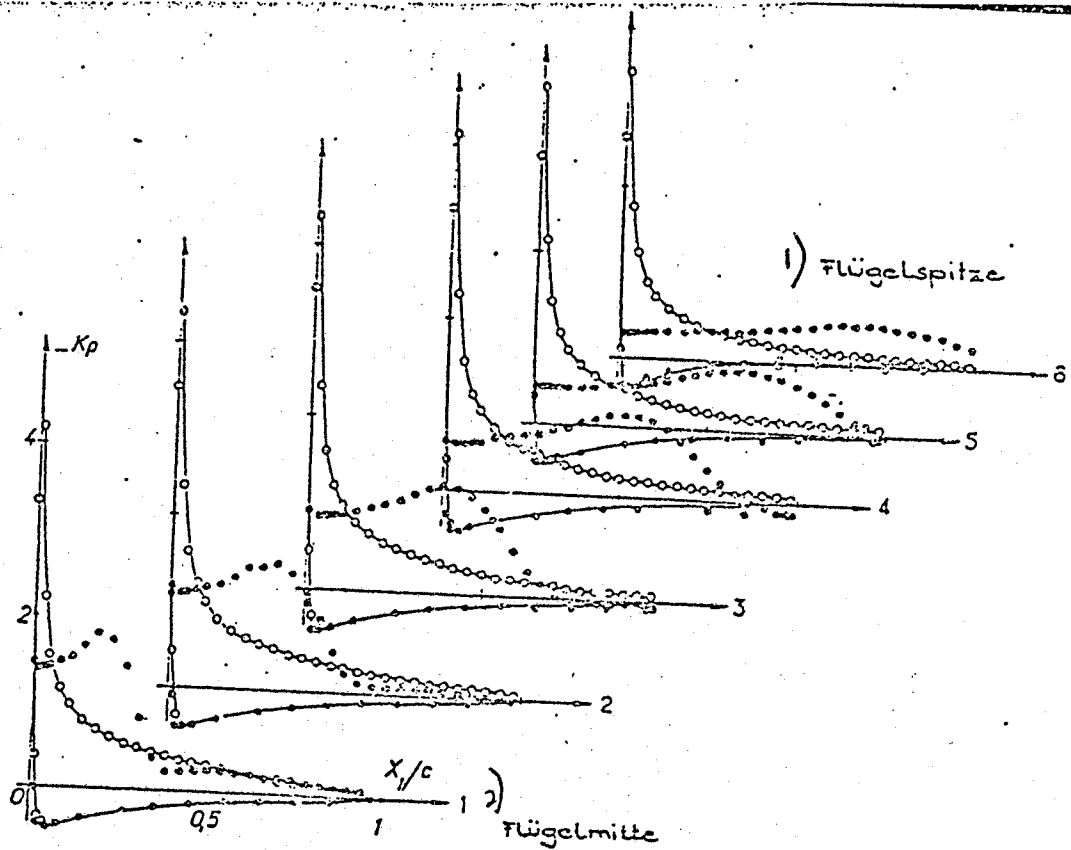


Figure 27 Flow Model for Partially Separated Flow on MF 3;  $\alpha \approx 16^\circ$

Key: 1) Flow Direction in ----- Vortex Sheet  
 in - - - - - Boundary Layer 2) Separating Line 3)  
 Reattachment Line 4) Rolling up Process of the Vortex  
 Sheet



•  $Re = 0.84 \cdot 10^6$   
 •  $Re = 1.92 \cdot 10^6$   
 $\varphi = 50^\circ ; \alpha = 12^\circ$

**Figure 28** Pressure Distribution on an Arrowhead Wing with  $\varphi = 50^\circ$  at  $Re = 0.84 \times 10^6$ ; from [12]  
 Key: 1) Wing Tip 2) Wing's mid-span section 3) Line of Secondary Separation 4) Line of Reattachment

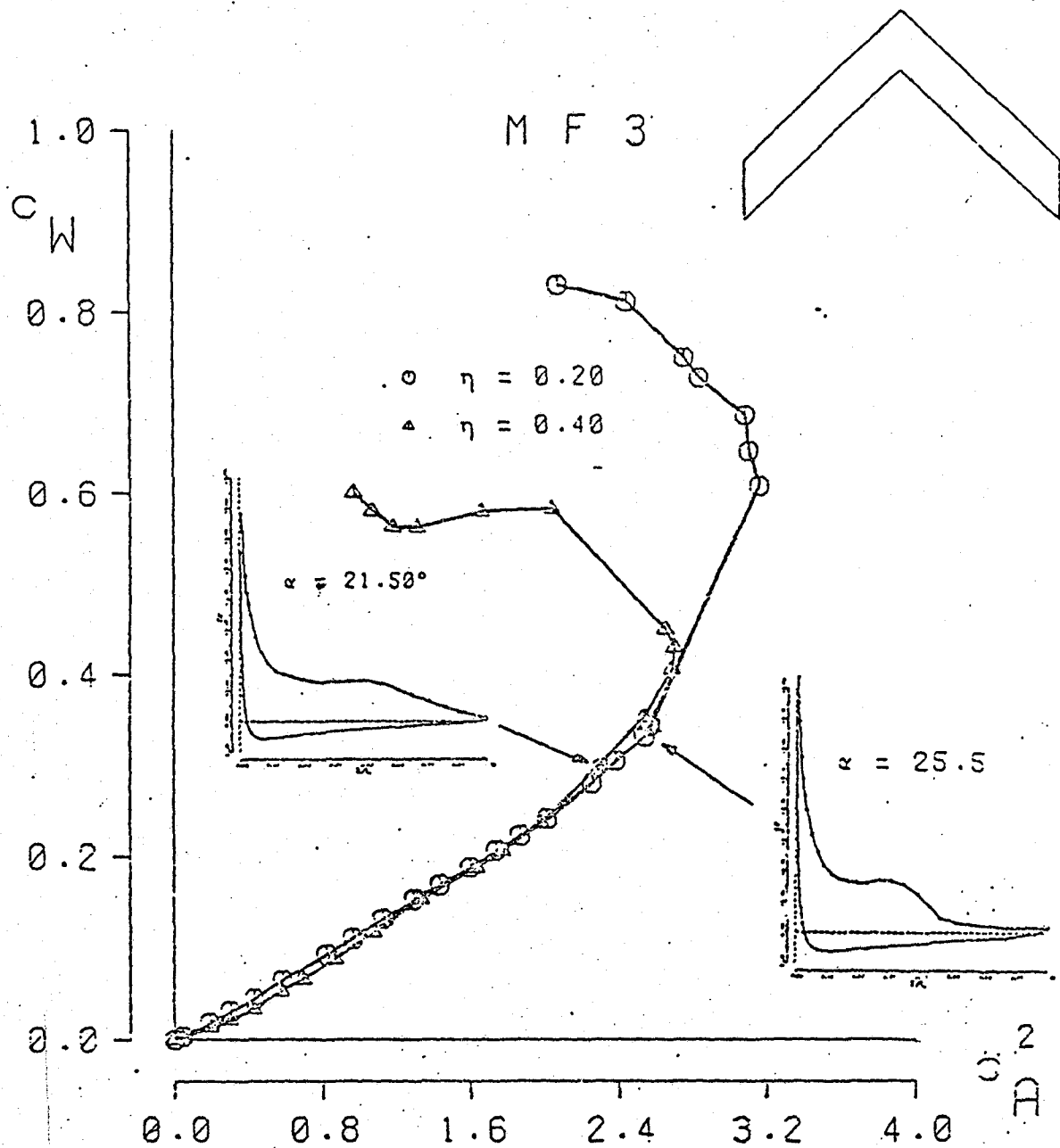
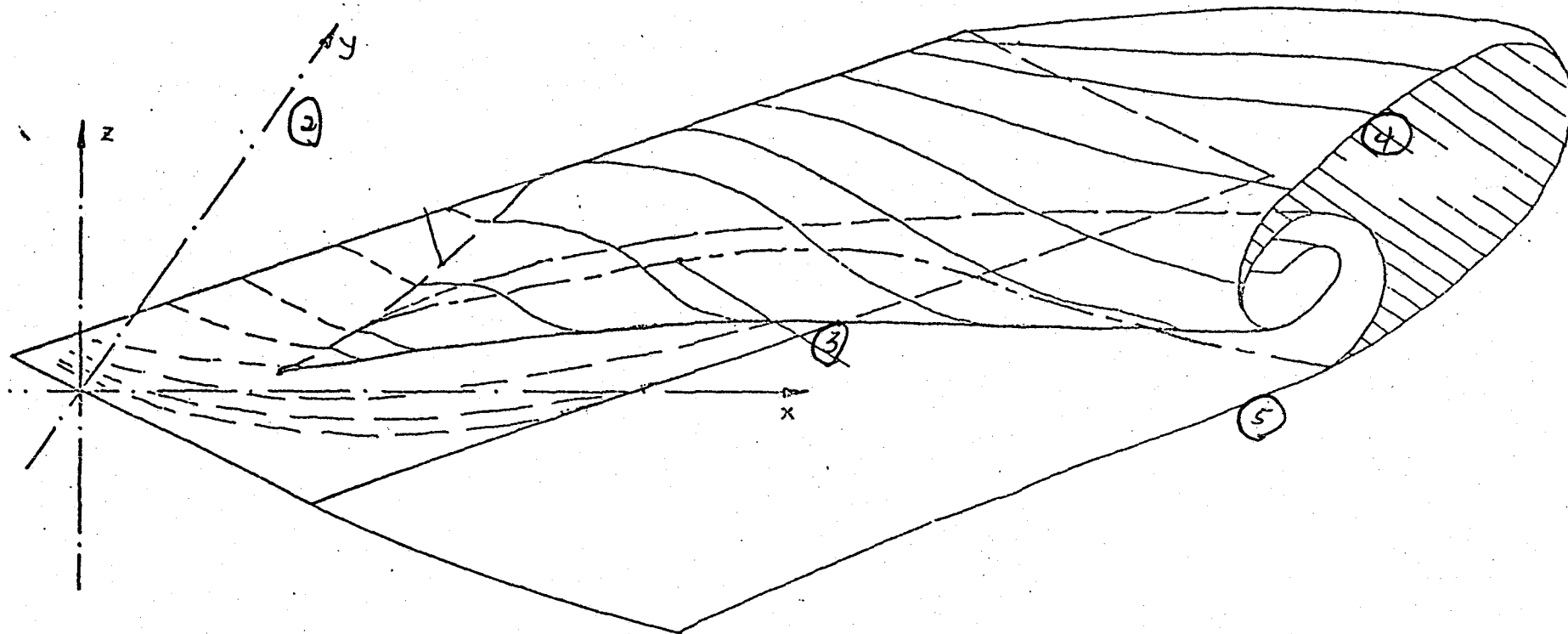


Figure 29 Function of  $c_w$  over  $c_A^2$  at  $\eta = 0.2$  and  $\eta = 0.4$ ; Wing MF 3



**Figure 30** Flow Model for Partially Separated Flow on MF 3;  $\alpha \approx 20^\circ$  to  $22^\circ$

Key: 1) Flow Direction in ----- Vortex Sheet  
 in - - - - - Boundary Layer 2) Separating Line 3)  
 Reattachment Line 4) Dead Water 5) Rolling up of the  
 Vortex Sheet

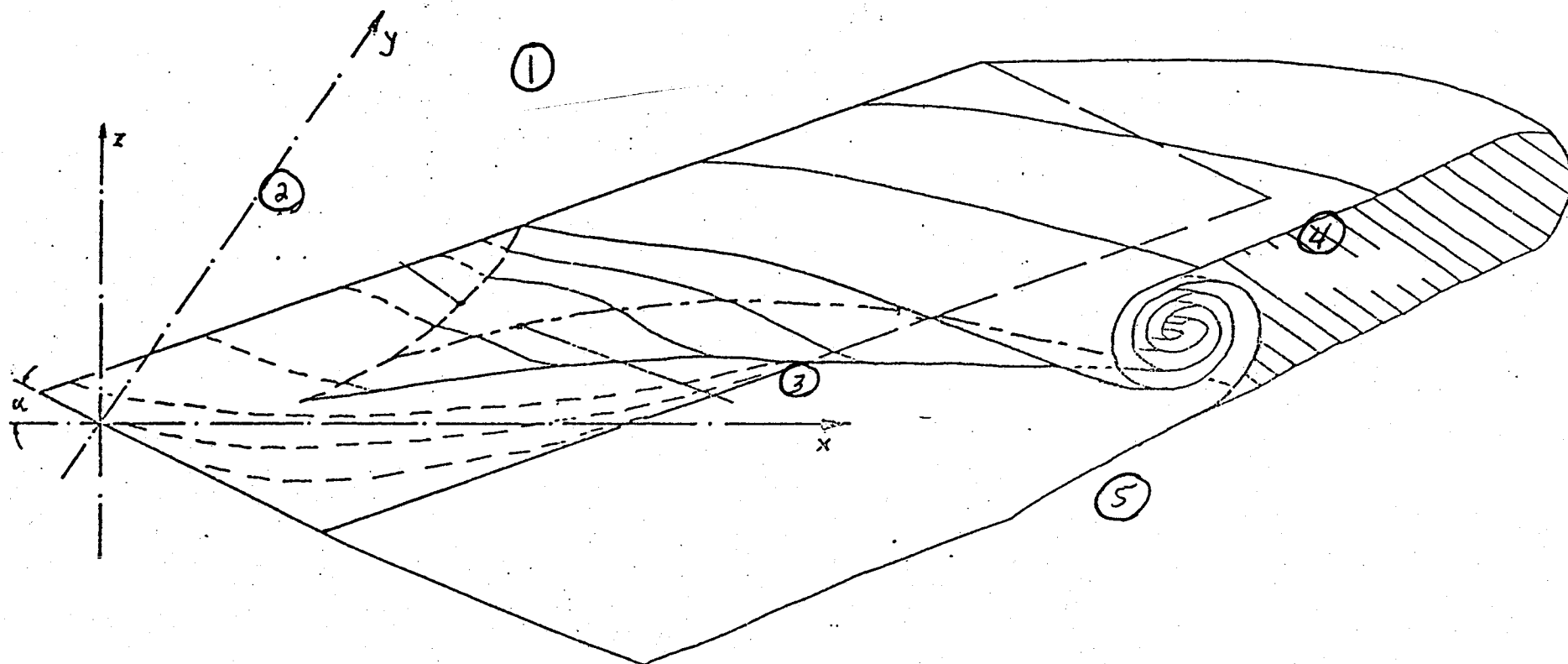


Figure 31 Alternative Flow Model for Partially Separated Flow on MF 3;  $\alpha \approx 20^\circ$  to  $22^\circ$

Key: 1) Flow Direction in ----- Vortex Sheet  
 in - - - - - Boundary Layer 2) Separating Line 3)  
 Reattachment Line 4) Dead Water 5) Rolling up of the  
 Vortex Sheet, 2 Vortex Systems

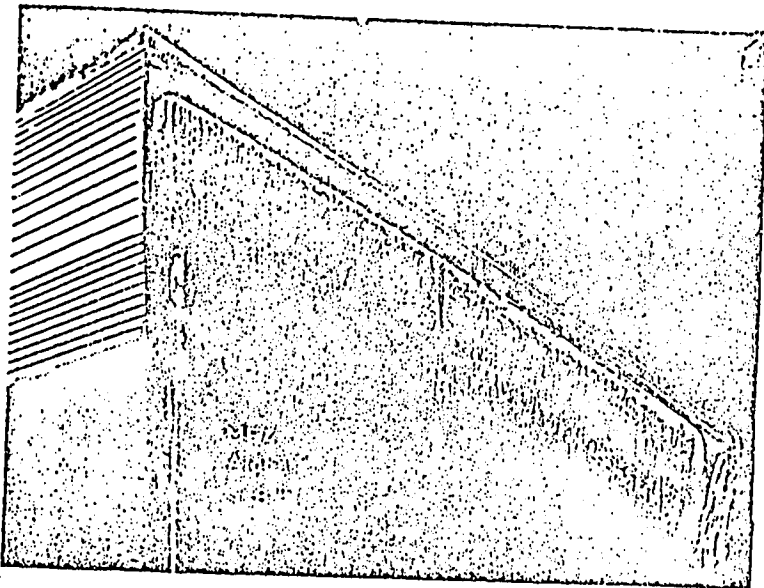


Bild 32

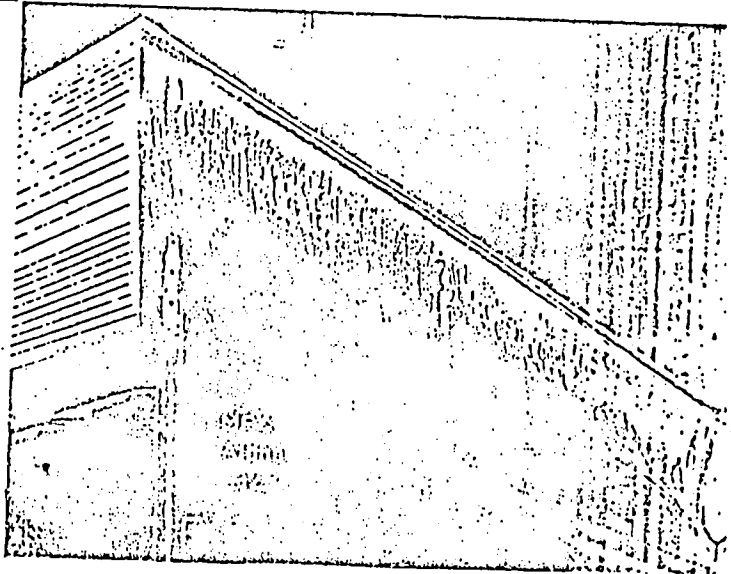


Bild 33

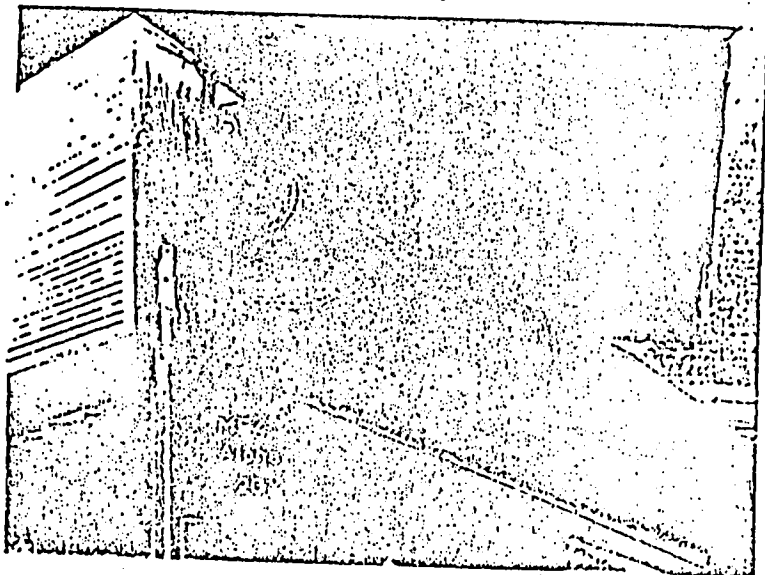


Bild 34

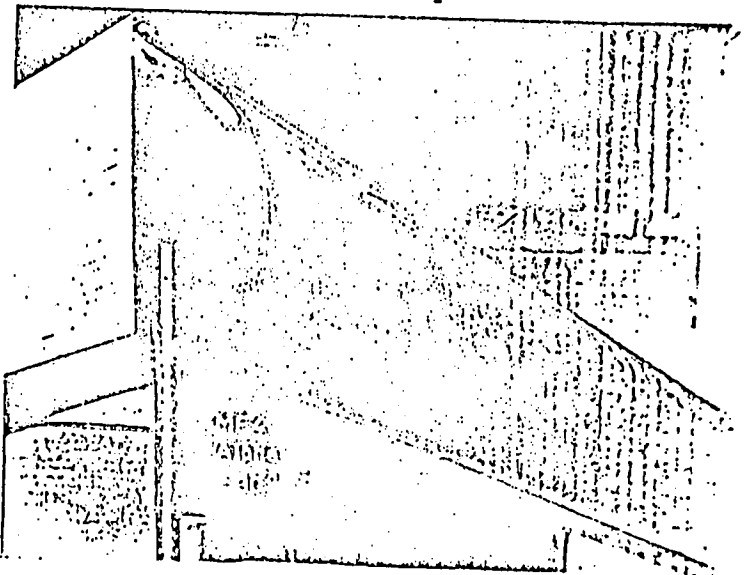


Bild 35

Figures 32 to 35 Representation of Tangential Wall Stress  
Pattern on the Wing's Upper Side with a Colored  
Process; Wing MF 4 ("Bild" = "Figure")

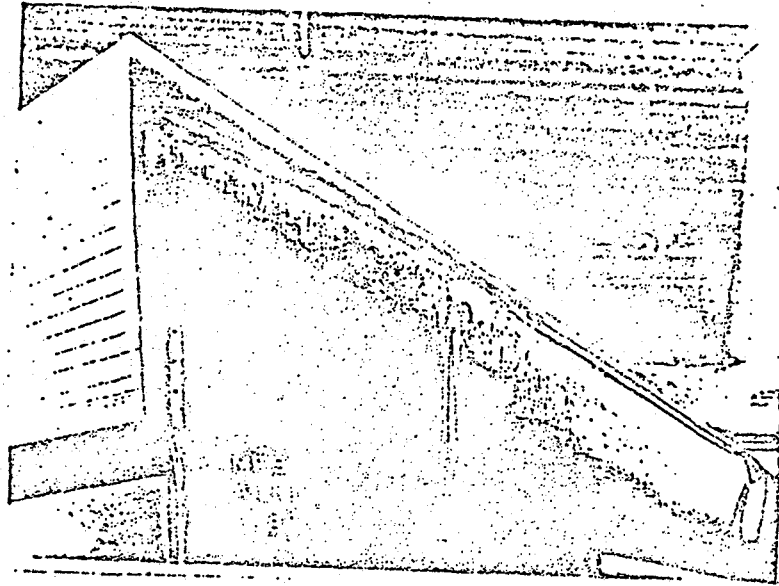


Figure 36 Representation of Tangential Wall Stress Pattern on the Wing's Upper Side with a Colored Process; Wing MF 5

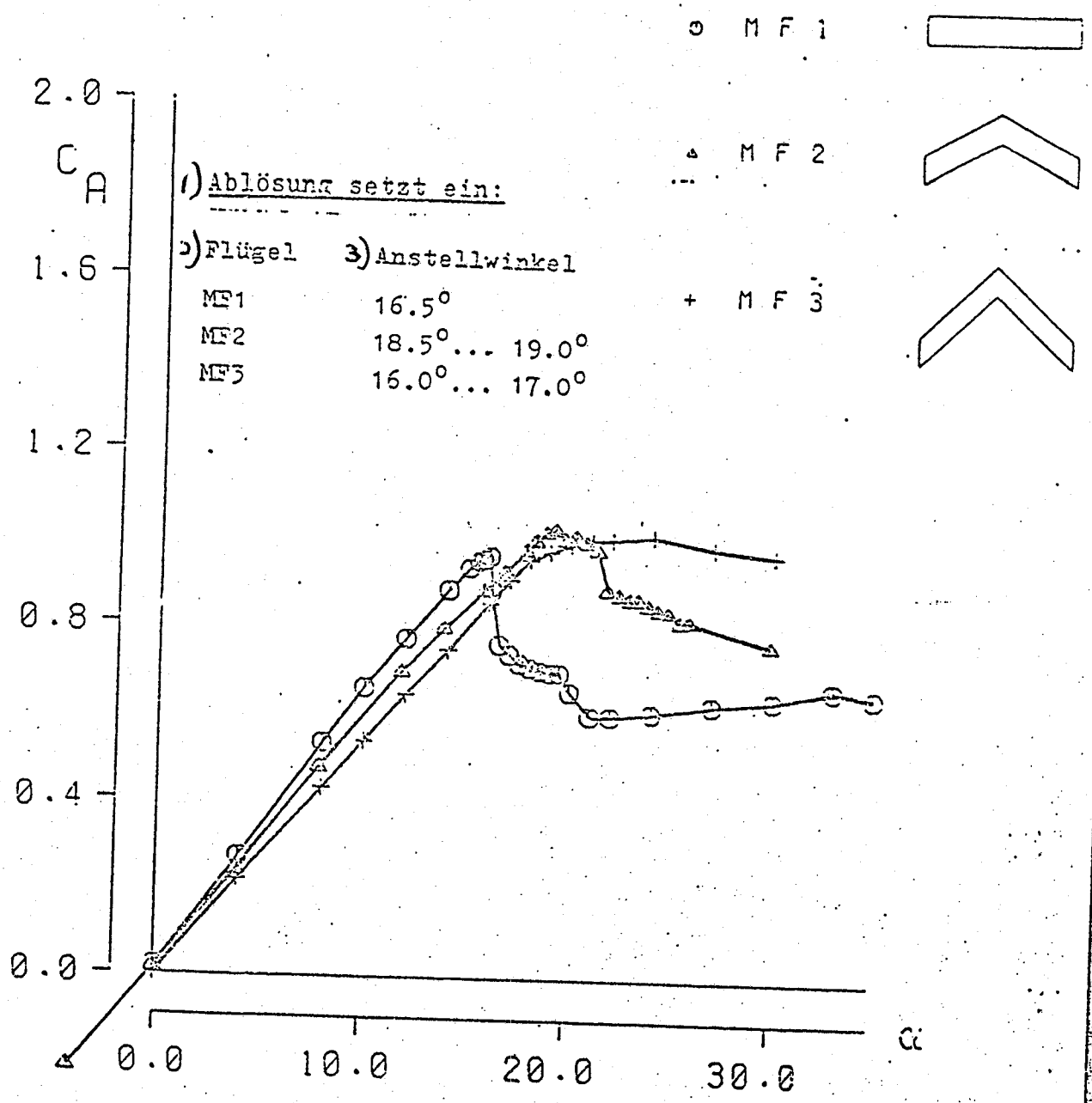


Figure 37 Comparison of  $C_A = f(\alpha)$  for Wings MF 1, MF 2, and MF 3  
 Key: 1) Separation begins 2) Wing 3) Angle of Attack

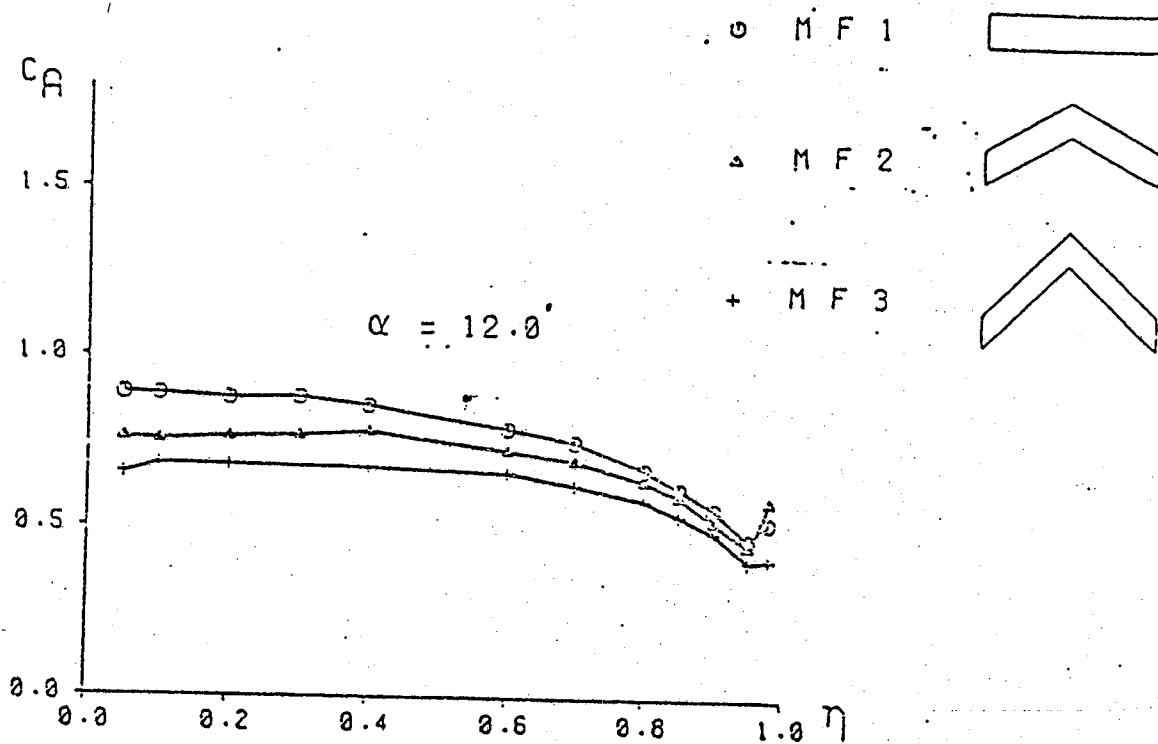


Figure 38 Comparison of Span Lift Distribution on Wings MF 1, MF 2, and MF 3

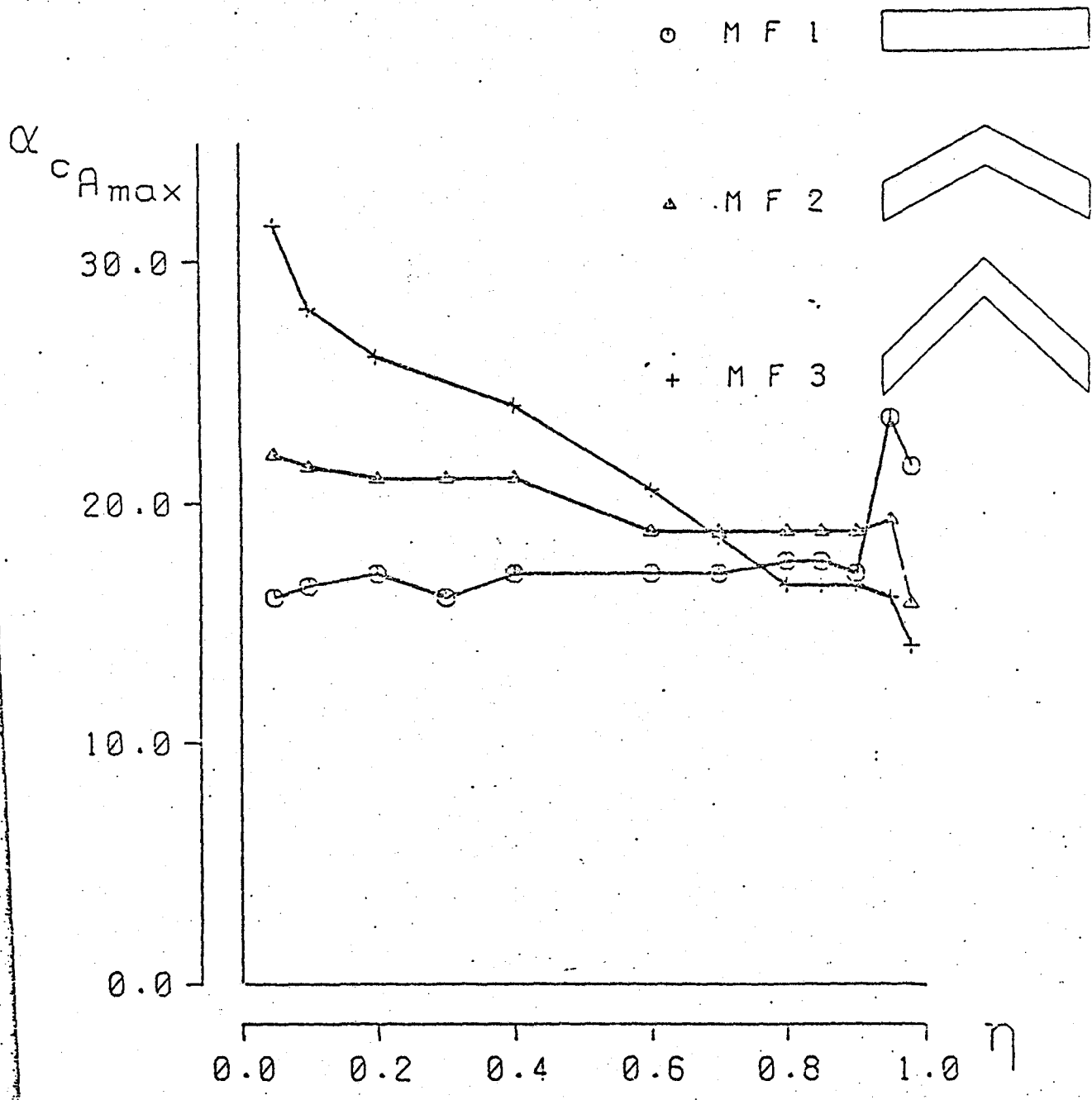


Figure 39  $\alpha_{cA_{max}} = f(\eta)$  for Wings MF 1, MF 2, and MF 3

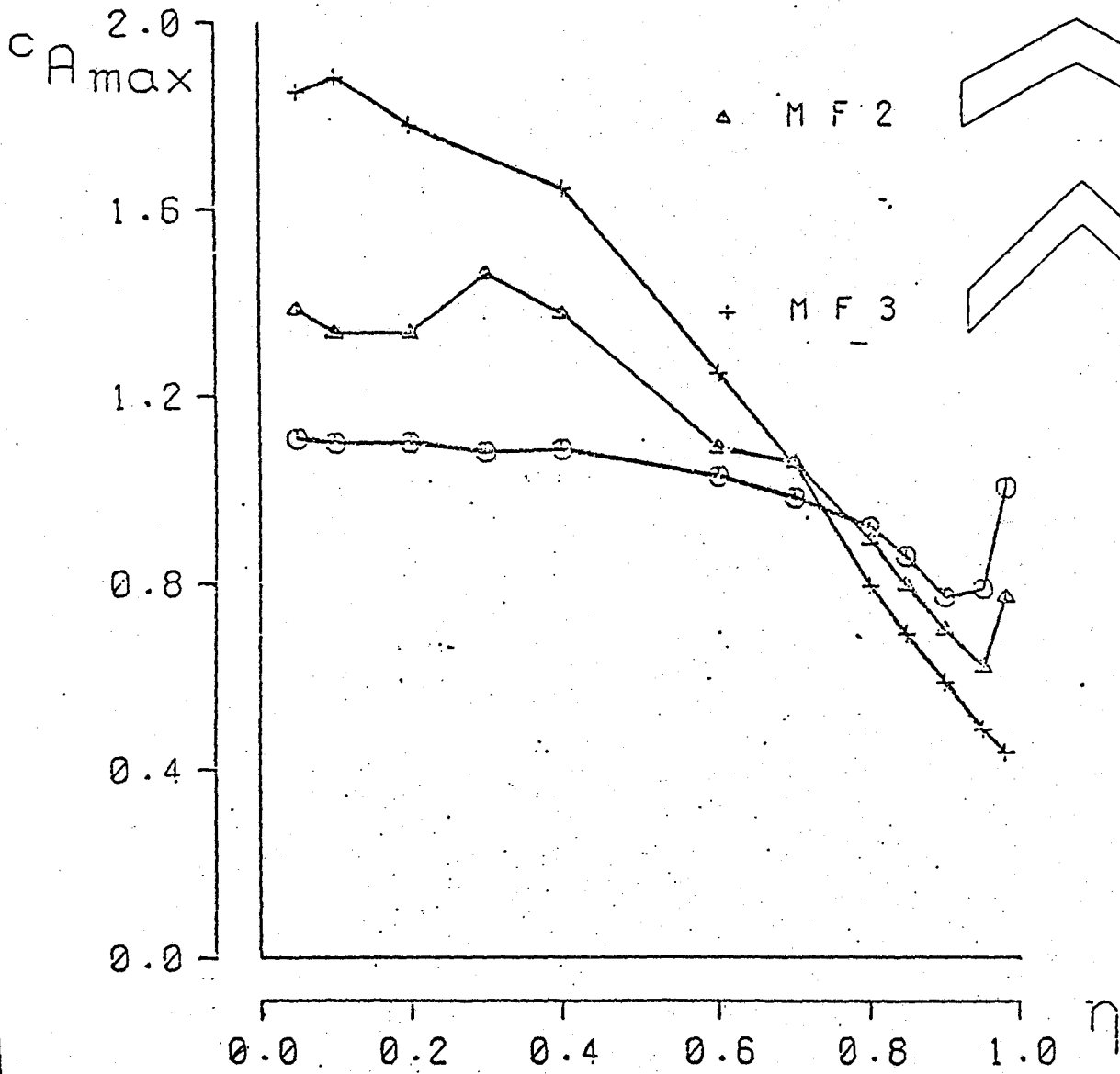


Figure 40  $c_{A_{max}} = f(\eta)$  for Wings MF 1, MF 2, and MF 3

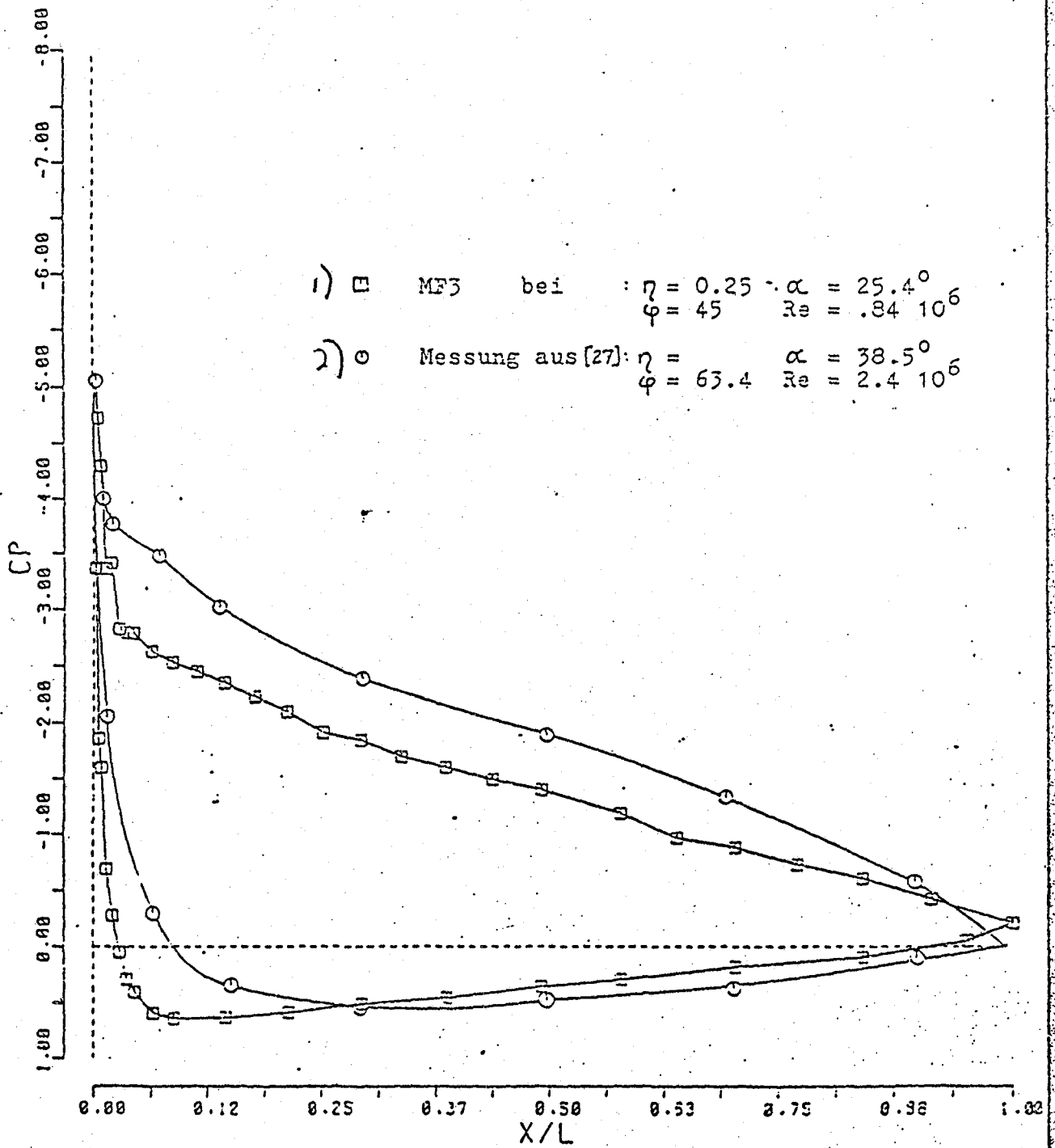


Figure 41 Comparison of a Pressure Distribution on Arrowhead Wing MF 3 with a Pressure Distribution on a Delta Wing  
 Key: 1) MF 3 at 2) Measurements from [27]

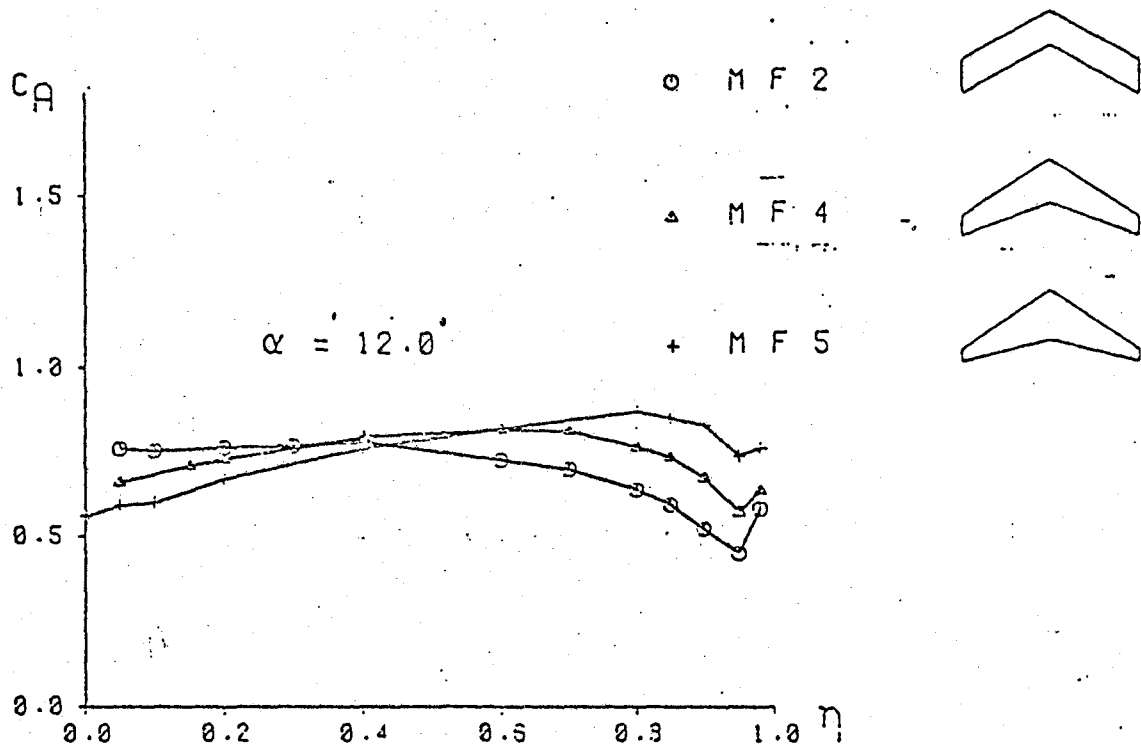


Figure 42 Comparison of Span Lift Distribution on Wings MF 2, MF 4, and MF 5

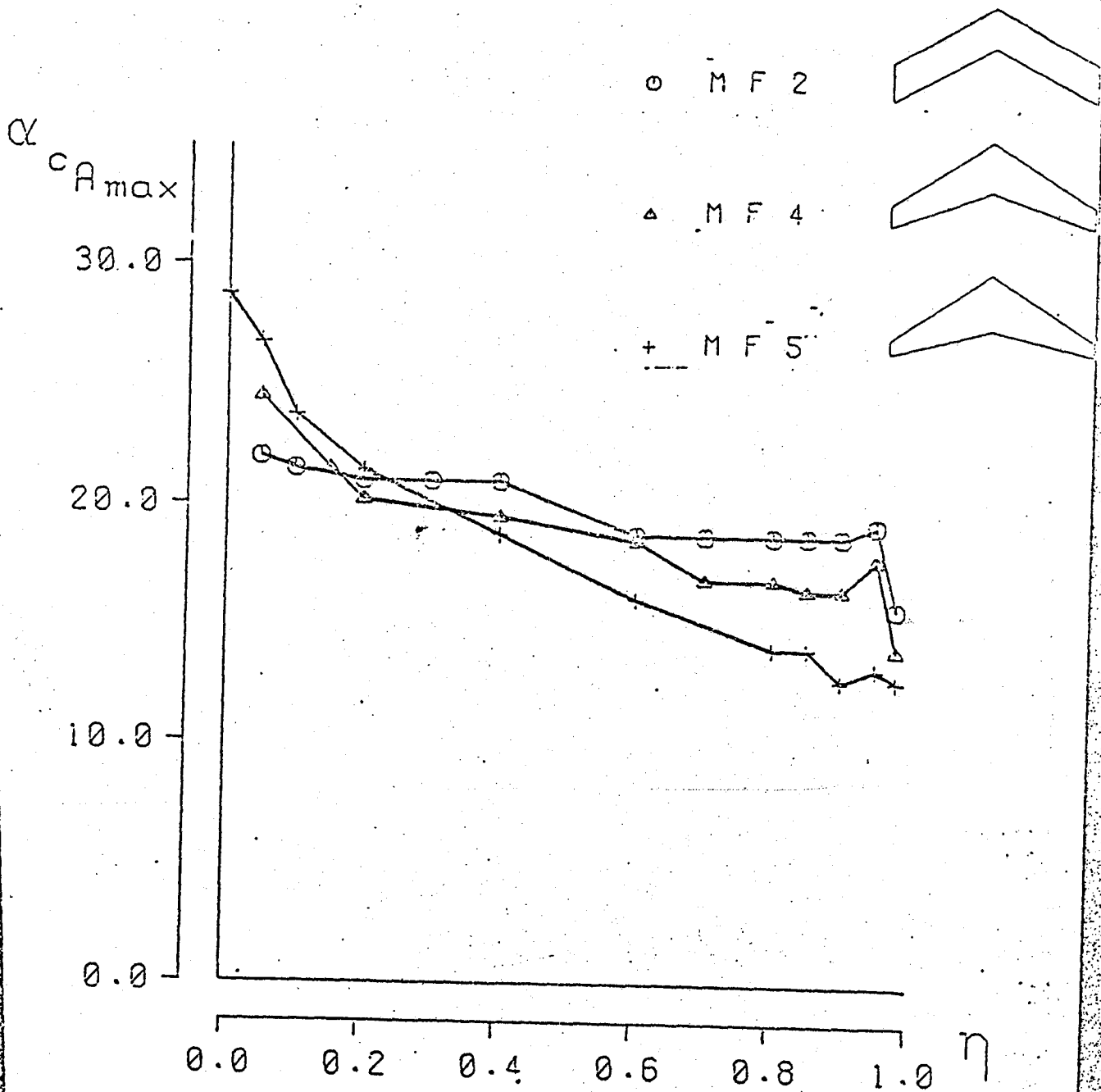


Figure 43  $\alpha c_{A_{max}} = f(\eta)$  for Wings MF 2, MF 4, and MF 5

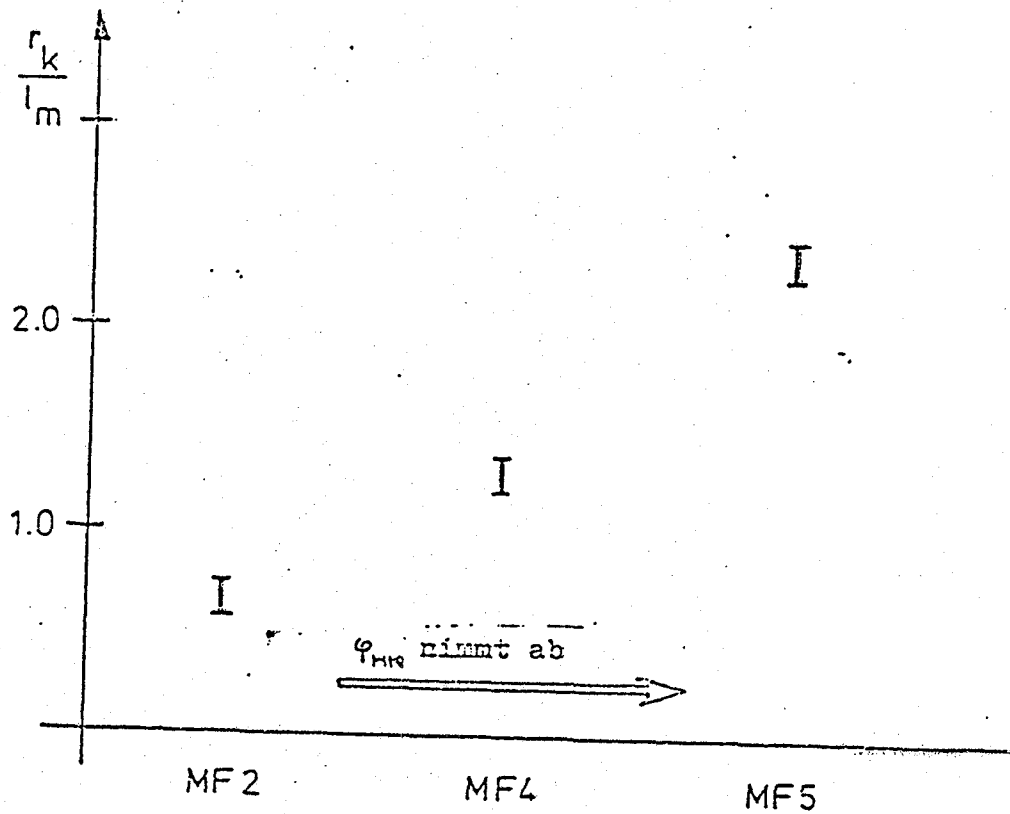
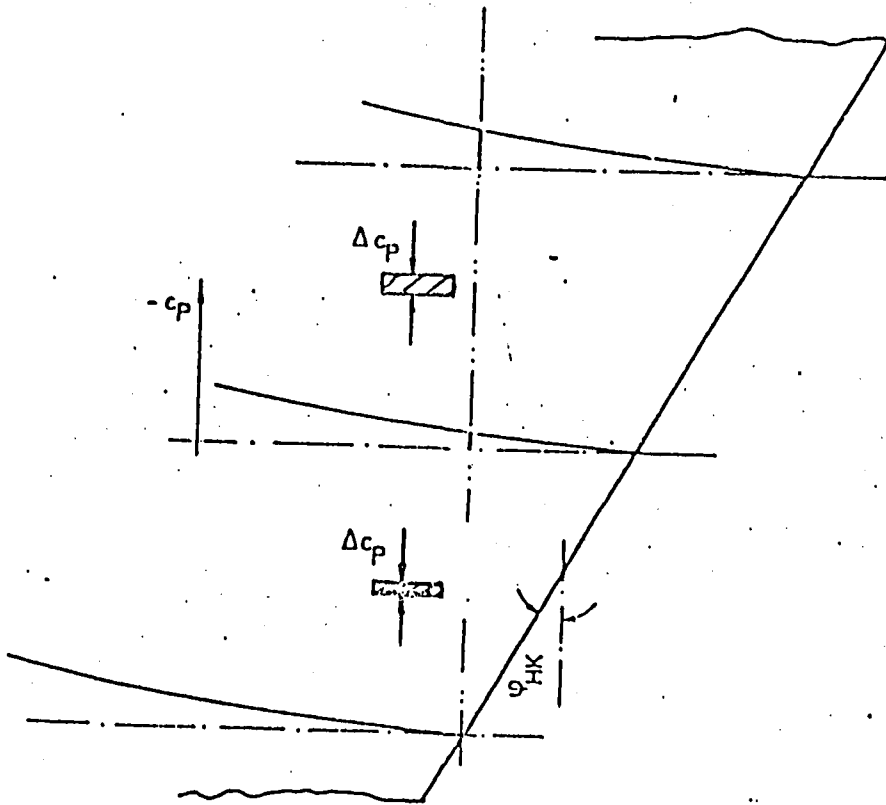
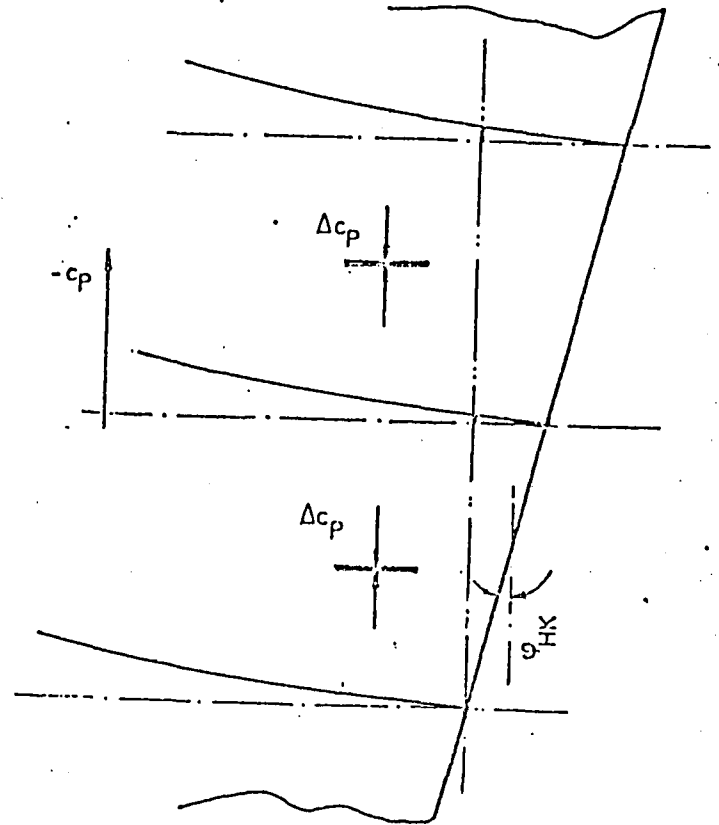


Figure 44 Curvature Radius of Wall Flow Line in Trailing Edge Region as a Function of Trailing Edge Sweep (for the Range  $\eta = 0.3$  to  $0.5$ )

Figure 45 Effect of Trailing Edge Sweep on Span Pressure Gradients



MF 2 ;  $\varphi_{HK} = 30^\circ$



MF 5 ;  $\varphi_{HK} = 12.26^\circ$

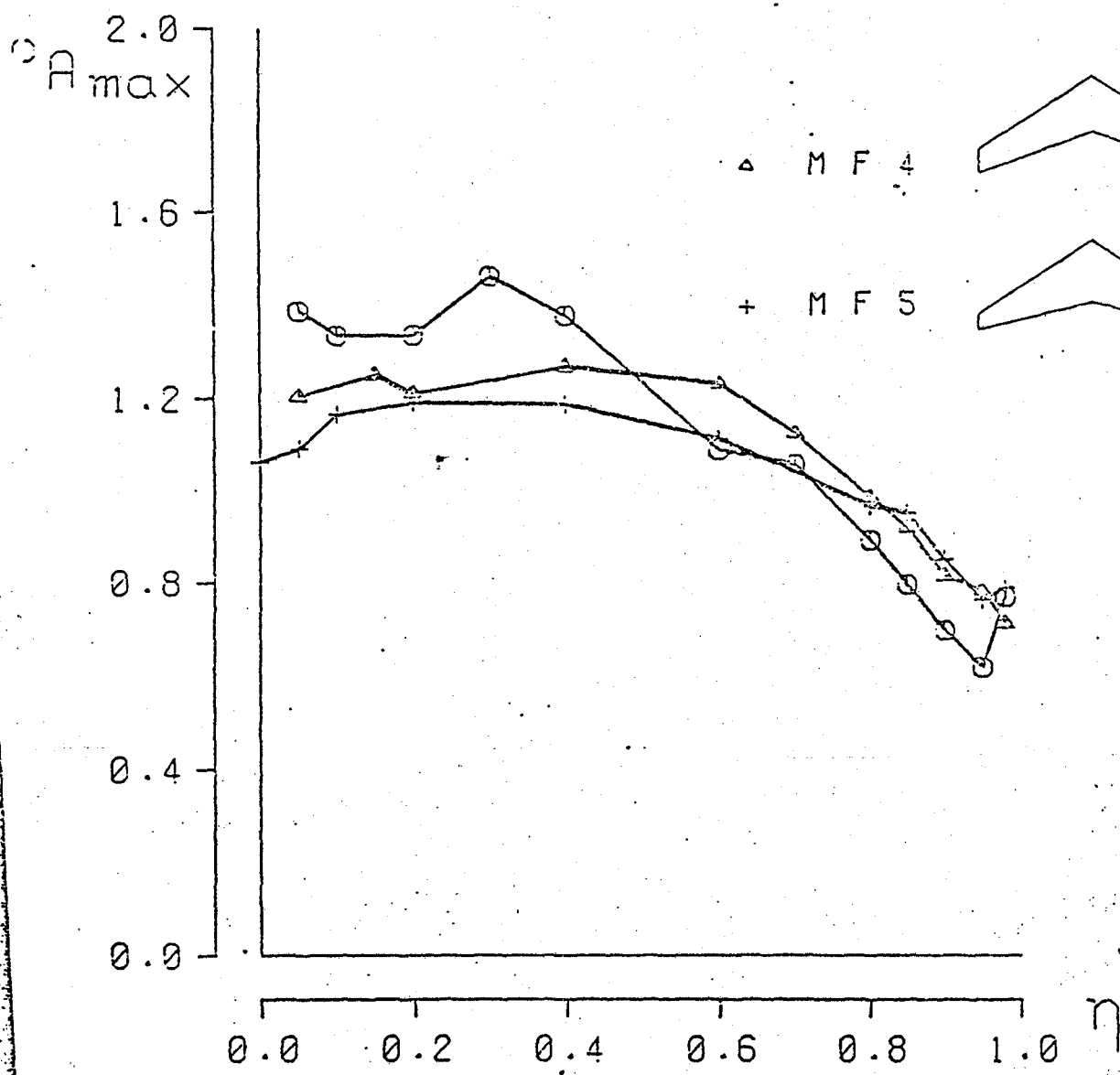


Figure 46  $c_{A_{max}} = f(\eta)$  for Wings MF 2, MF 4, MF 5

LANGLEY RESEARCH CENTER



3 1176 00188 5715